RSC Advances

This article can be cited before page numbers have been issued, to do this please use: S. Banerjee, P. Brandao and A. Saha, *RSC Adv.*, 2016, DOI: 10.1039/C6RA21217D.

ROYAL SOCIETY OF CHEMISTRY

www.rsc.org/advances

View Article Online
DOI: 10.1039/C6RA21217D

A Robust Fluorescent Chemosensor for Aluminium Ion Detection Based on Schiff base Ligand with Azo Arm and Application in Molecular Logic Gate

Saikat Banerjee,[a] Paula Brandão[b] and Amrita Saha[*a]

[a]*Department of Chemistry, Jadavpur University, Kolkata- 700032, India.*

E-mail: asaha@chemistry.jdvu.ac.in; amritasahachemju@gmail.com; Tel. +91-33-24572941

[b]*TEMA−NRD, Mechanical Engineering Department, University of Aveiro, 3810-193 Aveiro, Portugal*

Abstract

In this present work we reported synthesis and structural characterisations of a N2O2 donor Schiff base chemosensor with azo arm (**H_2L**). Various spectroscopic tools like single crystal X-ray, NMR, UV-vis, FTIR, ESI-Mass etc have been deployed to develop the present work. In recent past years a number of azo derived chemosensors have been reported by different research groups. This is first time we are reporting designing and properties of an azo derived chemosensors (**H_2L**) for detection of aluminium ion in semi aqueous medium. It has been found that it selectively senses Al^{3+} ion in semi aqueous solution. Here, the sensing process is mainly based on Chelation enhanced fluorescence process (CHEF). It has very high selectivity over other metal ions and anions. A detailed literature survey has been carried out and compared with this work. It has appreciably low detection limit i.e. 6.93 nM.^{1}HNMR titration was done to support the plausible complexation process. 1:1 stoichiometry binding between the chemosensor and Al^{3+} ion has been confirmed from Job's plot. An inhibition molecular logic gate has been constructed using Chemosensor (**H_2L**), where Al^{3+} and EDTA act as inputs and Fluorescence

View Article Online
DOI: 10.1039/C6RA21217D

emission as output. The structural and electronic parameters of the chemosensor (**H_2L**) and complex $[AL(L)]NO_3$ have been studied in details using theoretical tools like DFT and TDDFT.

Introduction

The design and construction of powerful and highly selective fluorescent chemosensors have attracting considerable attention in biomimetic chemistry.[1] Among various heavy metal ions Aluminium is an essential element due to its abundance and use in every sphere of life as utensils, electronic and electrical components of different gadgets, building equipment, different packaging items, water treatments, food additives, pharmaceutical products, occupational dusts etc. Aluminum is a known neurotoxin to organisms[1] and is believed to cause Alzheimer's disease,[2] osteomalacia[3] and breast cancer.[4] Toxicity due to the presence of excess aluminium in human health may arise as it inhibits several essential elements of similar size and charge like Mg^{2+}, $Ca^{2+}$and Fe^{3+}. It is also responsible for retarded growth of plants[5] and oxidative damage of the cell membrane.[6] In spite of its many drawbacks, the enormous use of Al in daily life causes accumulation of Al^{3+} and hence toxicity towards human health and the environment. WHO recommended the average weekly human body dietary intake of Al^{3+} of around 7 mg/kg body weight.[7] Thus, it is utmost urgent to detect Al^{3+} ion in environment in trace level i.e. in ppb, ppm or nano level. Unfortunately, the determination of Al^{3+} is complicated mainly due to its poor coordination ability, strong tendency to hydration, and lack of suitable spectroscopic characteristics.[8] Some analytical methods are available for detection of Al^{3+} such as graphite furnace atomic absorption spectrometry, inductively coupled plasma atomic emission spectrometry, atomic absorption spectra,[9] electrochemistry,[10] mass spectrometry,[11] and ^{27}Al NMR technology.[12] Most of them are expensive and time consuming. Optical detection

View Article Online
DOI: 10.1039/C6RA21217D

particularly fluorescence spectroscopic technique is advantageous over the other techniques because of its operational simplicity, low cost, low detection limit, real-time detection, selectivity, time saving and environmental friendly property. Therefore design and synthesis of new chemosensor for the detection of Al^{3+} has received considerable attention. Recently various research groups have reported different organic probes which can selectively detect Al^{3+}.[13,14] Although example of such Al^{3+} detecting chemosensors are still less compared with other metal ions detecting chemosensors like Zn^{2+} mainly due to less coordinating ability of Al^{3+} compared to other metal ions. Therefore, more improvement in this field is still required. Current literature survey (Table S1) reveals that preparation of most of the chemosensors for detection of Al^{3+} involves expensive stating materials, multiple reaction steps, use of different solvent mixtures and maintenance of drastic reaction conditions i.e. very high or low temperature, presence of catalyst etc. G. Das and *et al*. in a recent work[14n] have reported an Al^{3+} sensing organic probe viz. (E)-N'-((E)-3-(4-(dimethylamino)phenyl)allylidene)picolinohydrazide using starting materials picolinohydrazide and 4-(dimethylamino)cinnamaldehyde. Preparation of picolinohydrazide involves multiple steps. Preparation of another chemosensor viz. 2-((naphthalen-6-yl)methylthio)ethanol involves inert atmosphere and finally the product has been purified through column chromatography with 65% yield.[14e] S. Goswami and coworkers have reported a spirobenzopyran-quinoline (SBPQ) based sensor which selectively detects Al^{3+} along with Fe^{3+} and Cr^{3+}. Preparation of this type of chemosensors also involves multiple steps.[14o] It is also important to mention that 2-hydroxynapthaldehyde based organic probes are mostly used for fluorescence sensing ofAl^{3+}.[14p]

Different mechanistic pathway like intramolecular charge transfer (ICT),[15] photo induced electron transfer (PET),[16] chelation-enhanced fluorescence (CHEF),[17] metal−ligand charge

View Article Online
DOI: 10.1039/C6RA21217D

transfer (MLCT),[18] excimer/exciplex formation, imine isomerization,[19] intermolecular hydrogen bonding,[20] excited-state intramolecular proton transfer,[21] displacement approach,[22] and fluorescence resonance energy transfer[23] are adopted to explain the action of different fluorescence probe. Among different types of chemosensors, Schiff bases incorporated with different functionalized moiety are widely used mainly due to their ease of synthesis and low cost.

In this work an azo based salen-type of Schiff base ligand (E)-6,6'-((1E,1'E)-(propane-1,3-diylbis(azanylylidene))bis(methanylylidene))bis(2-methoxy-4-((E)-phenyldiazenyl)phenol) (**H_2L**) is structurally characterized and it exhibit high selectivity towards Al^{3+}(3.31×10^3 M^{-1}) with low detection limit (6.93 nM). Azo derivatives have prevalent use in different fields like pharmaceuticals, optical data storage, non-linear optics, photo switching devices, textile industry dye-sensitized solar cells and they also act as fluorescent chemosensors.[24-30] Our work is important and novel in this aspect because although various azo containing chemosensors are reported in literature but to the best of our knowledge in this work we are first time reporting one such sensor which can selectively detect Al^{3+}. Our organic probe possesses some extra advantages. We have prepared **H_2L** using easily available starting materials. The azoaldehyde was prepared from well known easy diazotization process with very high yield. The azoaldehyde upon reaction with a simple diamine produced **H_2L** with >90% yield. We have successfully isolated both the azoaldehyde and Schiff base **H_2L** in highly crystalline form. The ligand is characterized by different techniques including x-ray crystallography. The composition of the Al^{3+}-ligand complex (Complex **1**) has been established by different spectroscopic data like IR, Mass, Job's plot and ^1H NMR. The DFT computation of optimized geometry of **H_2L** and the complex $[Al(L)]^+$ has been used to support the electronic spectral properties.

View Article Online
DOI: 10.1039/C6RA21217D

Experimental

Materials and Physical measurements

All reagent or analytical grade chemicals and solvents were purchased from commercial sources and used without further purification. Elemental analysis for C, H and N was carried out using a Perkin–Elmer 240C elemental analyzer. Infrared spectra (400–4000 cm^{-1}) were recorded from KBr pellets on a Nicolet Magna IR 750 series-II FTIR spectrophotometer. Absorption spectra were measured using a UV-2450 spectrophotometer (Shimadzu) with a 1-cm-path-length quartz cell. Measurements of NMR spectra were conducted using a Bruker 300 spectrometer in DMSO-d_6 and $CDCl_3$respectively. Emission was examined by LS 55 Perkin–Elmer spectrofluorimeter at room temperature (298 K) in HEPES buffer at pH= 7.4 solution under degassed condition. Fluorescence lifetimes were measured using a time-resolved spectrofluorimeter from IBH, UK.

Synthesis of (E)-5-(2-phenyldiazenyl)-2-hydroxy-3-methoxybenzaldehyde

4 mL conc. HCl was added to 15 mL water and kept in an ice bath keeping the temperature 0^0C. To it, aniline (4.0 mmol, 0.372 g) was added. To this mixture an aqueous solution of sodium nitrite (6.0 mmol, 0.414 g) was drop wise added over a time of 30 mins. The mixture was stirred for 1 h at 0^0C. Then the resultant solution was added to the alkaline *o*-Vanillin (4.8 mmol, 0.732 g) which is kept in another ice bath. The mixture was further stirred for 1 h at 0^0C. The solution was neutralised using dilute HCl and p^H was maintained around 7.0. The mixture was extracted with chloroform and evaporated to result red coloured crystals of the aldehyde.

View Article Online
DOI: 10.1039/C6RA21217D

Yield: 0.953 g (94%). Anal. Calc. for $C_{14}H_{12}N_2O_3$: C 64.65%; H 5.79%; N 16.34%. Found: C 64.36%; H 5.31%; N 16.17%.IR (cm^{-1}, KBr): υ(N=N) 1459 s;ν(C-H) 762 s. ESI-MS (positive) in MeOH: The base peak was detected at *m/z* = 279.00, corresponding to $[M+23]^+$.

^1H NMR ($CDCl_3$, 300 MHz) δ ppm: 4.01 ($-OCH_3$) (s, 3H), 7.25-7.35 (Ar-H) (m, 2 H), 7.74-7.86 (Ar-H) (m, 5 H), 10.02 (-CH=O) (s, 1H), 11.05 (-OH) (bs, 1H).

Synthesis of Schiff base ligand (H_2L)

A mixture of (E)-5-(2-phenyldiazenyl)-2-hydroxy-3-methoxybenzaldehyde (2.0 mmol) and 1,3-diaminopropane (1.0 mmol, 0.074 g) was heated to reflux for 4 h in methanol-chloroform solvent mixture (1:1, v/v). Upon slow evaporation of the solvent mixture deep red colored crystals were obtained.

Yield: 0.5282 g (96%). Anal. Calc. for $C_{29}H_{26}N_6O_2$: C 67.62%; H 5.49%; N 15.26%. Found: C 66.86%; H 5.31%; N 14.97%.IR (cm^{-1}, KBr): υ(C=N) 1648s; υ(N=N) 1455 s;ν(C-H) 764 s. ESI-MS (positive) in MeOH: The base peak was detected at *m/z* = 551.21, corresponding to $[M+1]^+$. UV-Vis, λ_{max} (nm), (ε ($dm^3mol^{-1}cm^{-1}$)) in Acetonitrile: 290 (4533) and 388 (5736).

^1H NMR ($CDCl_3$, 300 MHz) δ ppm:2.25 ($-CH_2$) (m, 1H), 3.82-3.84 ($-CH_2$) (bs, 2H), 4.01 ($-OCH_3$) (s, 3H), 7.42-7.90 (Ar-H) (m, 7 H), 8.43 (-CH=N) (s, 1H).

^1H NMR (DMSO-d_6, 300 MHz) δ ppm: 2.08 ($-CH_2$) (m, 2H), 3.74-3.82 ($-CH_2$, $-OCH_3$) (bs, 10H), 7.30-7.48 (Ar-H) (m, 8H), 7.66-7.74 (Ar-H) (m, 6H), 8.66 (-CH=N) (s, 2H).

^{13}C NMR (DMSO-d_6, 75 MHz) δ ppm: 31.46 ($-CH_2$), 56.34 ($-CH_2$), 118.22, 122.58, 126.93, 127.41, 129.08 and 130.47 (Ar-C), 165.38 (-CH=N) .

View Article Online
DOI: 10.1039/C6RA21217D

Synthesis of [Al(L)](NO$_3$) complex

A 2 ml methanolic solution of aluminium nitrate nonahydrate (1.0 mmol, 0.375 g) was added drop wise to 20 mL methanolic solution of **H$_2$L** (1.0 mmol, 0.551 g) followed by addition of triethylamine (2.0 mmol, ~0.4 mL) and the resultant reaction mixture was stirred for 4 h under nitrogen atmosphere. Then the resultant mixture was dried to powdered form and further characterizations were carried out.

Yield: 0.6246 g (98%). Anal. Calc. for $AlC_{29}H_{24}N_7O_5$: C 67.62%; H 5.49%; N 15.26%. Found: C 66.86%; H 5.31%; N 14.97%.IR (cm^{-1}, KBr): υ(C=N) 1646s; υ(N=N) 1545 s;ν(C-H) 770 s. ESI-MS (positive) in MeOH: The base peak was detected at *m/z* = 575.25, corresponding to $[Al(L)]^+$. UV-Vis, λ_{max} (nm), (ε (dm^{3}mol^{-1}cm^{-1})) in Acetonitrile: 286 (5083) and 375 (5949). ^{1}H NMR (DMSO-d$_6$, 300 MHz) δ ppm: 2.16 (-CH$_2$) (bs, 2H), 3.89-3.95 (-CH$_2$, -OCH$_3$) (bs, 10H), 7.54-7.81 (Ar-H) (m, 14H), 9.24 (-CH=N) (s, 2H).

X-ray crystallography

Single crystal X-ray data of azoaldehyde and Schiff base ligand (**H$_2$L**) were collected on a Bruker SMART APEX-II CCD diffractometer using graphite monochromated Mo Kα radiation (λ = 0.71073 Å) at room temperature. Data processing, structure solution, and refinement were performed using Bruker Apex-II suite program. All available reflections $2\theta_{max}$ were harvested and corrected for Lorentz and polarization factors with Bruker SAINT plus.[31] Reflections were then corrected for absorption, inter-frame scaling, and other systematic errors with SADABS.[32] The structures were solved by the direct methods and refined by means of full matrix least-square technique based on F^2 with SHELX-1997 and SHELX-2013 software package.[33] All the non-hydrogen atoms were refined with anisotropic thermal parameters. C-H

View Article Online
DOI: 10.1039/C6RA21217D

hydrogen atoms were inserted at geometrical positions with U_{iso} = 1/2U_{eq} to those they are attached. Crystal data and details of data collection and refinement are summarized in Table 1.

Computational method

All computations were performed using the GAUSSIAN09 (G09)[33] software package. Coordinates obtained from single crystal X-ray data were used for optimization of structure of Ligand (**H_2L**). For optimization we used the density functional theory method at the B3LYP level[35,36] and the standard 6-31+G(d) basis set for C, H, N and O atoms[36,38] and the lanL2DZ effective potential (ECP) set of Hay and Wadt[39–41] for aluminum atom have been chosen for optimization .

TDDFT calculation was performed with the optimized geometry to ensure only positive eigen values. Time-dependent density functional theory (TDDFT)[42–44] was performed using conductor-like polarizable continuum model (CPCM)[44–47] and the same B3LYP level and basis sets in aqueous solvent system. GAUSSSUM[48] was used to calculate the fractional contributions of various groups to each molecular orbital.

Results and discussion

Synthesis and Characterization

The azoaldehyde5-(2-phenyldiazenyl)-2-hydroxy-3-methoxybenzaldehyde is synthesized by first diazotization of primary aromatic amine (aniline) followed by coupling with an aromatic alcohol (o-vanillin). Azoaldehyde reacted with 1,3-diamino propane in 2:1molar ratio at ambient temperature in methanol to generate the Chemosensor **H_2L** (Scheme 1). The yield of both the aldehyde and **H_2L** is >90%. Both of them are crystallized from slow evaporation of methanol-chloroform (3:5) mixture. They are well characterized by ^{1}H NMR, ^{13}C NMR, mass and IR

View Article Online
DOI: 10.1039/C6RA21217D

spectroscopy. In IR spectrum, azo (N=N) band of both azoaldehyde and **H_2L** appear at 1459 cm^{-1} and 1455 cm^{-1}respectively (Fig. S1). Other important stretching vibrations of **H_2L** are 1648 (s, υ(C=N)); 3100 cm^{-1} (υ(-OH)); 764 cm^{-1} (ν(C-H)) respectively. Similar characteristic stretching frequencies of $[Al(L)]NO_3$ are obtained at 1646 (s, υ(C=N)); 1530cm^{-1} (υ(N=N)); 770 cm^{-1}(ν(C-H)), respectively (Fig. S2). In complex **1**, nitrate ion is present as a counter anion. The characteristic stretching frequencies are obtained at 765 cm^{-1} (planar rock), 815 cm^{-1} (NO, deformation) and 1375 cm^{-1} (NO, asymmetric stretch), respectively, which are comparable with that of previously reported literature values.[49] In ^{1}H NMR spectrum of azoaldehyde ($CDCl_3$ solvent), aldehyde proton (-CH=O) appeared at 10.02 ppm whereas –OCH_3 and phenolic –OH protons appeared at 4.01 ppm and 11.05 ppm respectively. Azoaldehyde contains two aromatic rings. Aromatic protons came as multiplate at two different regions i.e. from 7.25 to 7.35 ppm and from 7.74 to 7.86 ppm respectively. In case of the **H_2L** ($CDCl_3$ solvent), aromatic protons appear around 7.74-7.30 ppm whereas azomethine proton, -OCH_3 protons and aliphatic protons appeared at 8.43, 4.01, 3.95and 2.25 ppm respectively. Here, Phenolic –OH proton is so labile that it becomes very difficult to arrest in both $CDCl_3$ and DMSO-d_6 solvent system. In ^{13}C spectra of **H_2L** (DMSO-d_6 solvent), aliphatic carbon signals appeared at 31.46 ppm and 56.34 ppm respectively, whereas aromatic carbons appeared in the region of 118 ppm to 130 ppm. The signal at 165 ppm is the characteristic signal for imine carbon (>C=N) (Fig. S3-S6). Mass spectral analysis of starting azoaldehyde and **H_2L** exhibit *m/z* peaks at 279.00 and 551.21, respectively (Fig.S7-S9). Mass spectrum of **H_2L** in the presence of Al^{3+}shows peak *m/z* at 575.25 which is corresponding to $[(Al(L)]^+$ (Fig. S10).

The structure of both azoaldehyde and **H_2L** has been established by single crystal X-ray diffraction measurement. Crystals of both the organic compound are obtained from slow

View Article Online
DOI: 10.1039/C6RA21217D

evaporation of CH_2Cl_2-CH_3OH solvent mixture. The ORTEP plot of azoaldehyde and **H_2L** are shown in Fig. 1 and Fig. 2 respectively and the selected bond parameters are listed in Table 2. The azoaldehyde crystallizes with a monoclinic space group Cc. It has almost planer structure where the azo nitrogen atoms and the aromatic ring containing –CHO, -OCH_3, -OH groups belong in the same plane. The remaining aromatic ring deviates from the plane to a small extent (10.71°). The N=N and C=O (-CHO) bond distances are 1.252Å and 1.224Å respectively which are similar with other reported values.[50] Aromatic C-C bond distances observed around 1.368 - 1.404 Å. In solid state it form 2D network through intermolecular hydrogen bonding between the phenoxy o-atom and aromatic hydrogen atom and edge to edge π-π stacking interaction between two phenyl rings. The distances are 2.704 Å and 3.70 Å respectively (Fig. S11).

The Schiff base ligand (**H_2L**) crystallizes with a triclinic space group $P\bar{1}$. The azo -N=N- bond distances are 1.217 Å and 1.268 Å respectively. The average C=N- bond distance is 1.287 Å. The C-C bond distances of the phenyl rings found around 1.342-1.472 Å, whereas aliphatic C-C bond distances appear around 1.511-1.531 Å. The propylenic part of the Schiff base, N3–C15–C16–C17–N4, is to some extent puckered due to the sp^3 hybridization of the saturated portion of the ligand. The bond angle (C15–C16–C17, 114.35(6)° deviates appreciably from its ideal value. OH group of the both of phenyl ring are placed 180° apart from each other to minimize the dipole-dipole interaction. In the Schiff base ligand each azo nitrogen atoms, imine atoms and the aromatic ring containing –CHO, -OCH_3, -OH groups belong in the same plane. The remaining aromatic ring deviates from the plane significantly by an angle of 83.03°.The molecule dimerizes in solid state through intermolecular H-bonding between the two –OH groups as well as between the –OH group and imine nitrogen atom. –O-H…O bond distance is 3.879Å whereas –O-H…N (imine) bond distance is 2.357Å (Fig. S12).

View Article Online
DOI: 10.1039/C6RA21217D

Structural parameters are again calculated from optimized structure using DFT where bond distances are marginally elongated by 0.0023–0.0435 Å and bond angles varies within the range of 0.05–1.39° (Table 2) compare with the X-ray crystallographic data. Therefore, the optimized results are helpful to explain the electronic structure and electronic properties of the ligand **H_2L**.

Absorption study

The UV–Vis spectrum of the Chemosensor **H_2L** was recorded at 25°C in aqueous buffer-acetonitrile solution (1:100 v/v, HEPES buffer at pH 7.4) which exhibited well-defined bands at 290 and 388 nm respectively. In order to study the binding property of **H_2L** toward Al^{3+} ion, UV–Vis spectra of **H_2L** (10 μM) in the presence of various concentrations of Al^{3+} (0–10 μM) were recorded at room temperature, as shown in Fig. 3. It has been observed that old peaks disappear and two new absorption bands emerge at 286 and 375 nm respectively, and its absorbance gradually increases with the gradual addition of Al^{3+} and it gets saturated upon addition of 1.0 equivalents of Al^{3+} keeping the concentration of **H_2L** fixed at 10 μM. These observations indicate the coordination of **H_2L** with one eq. of Al^{3+}(Fig. 3).

Al^{3+} ion sensing by fluorescence studies

The fluorescence property of **H_2L** was also investigated in HEPES buffer solution at pH 7.4 at room temperature. The ligand, **H_2L**, emits weakly at 510 nm when excited at 388 nm and the fluorescence quantum yield is (Φ= **H_2L**) 0.00939. Upon excitation at 290 nm we observed similar emission at 510 nm. Low fluorescence intensity of free **H_2L** probably due to photo induced electron transfer process (PET) caused by electron delocalization from the two phenoxido oxygen atoms to the π-conjugated system of two aromatic rings, >C=N– group and azo (-N=N-) group. Here presence of extended delocalization through azo group (-N=N-)

View Article Online
DOI: 10.1039/C6RA21217D

initiates appearance of fluorescence pick at 510 nm. After gradual addition of Al^{3+} ion with various concentrations (0-10 μM), a significant changes in emission spectra have been noticed. In presence of metal ion the emission band of **H_2L** is blue shifted to 478 nm. This result also confirms a high sensitivity of the receptor towards Al^{3+}. A plot of fluorescence intensities at 478 nm (I_{478}) vs concentration of aluminum has been given in Fig. 4. : inset. It shows that sensing character of **H_2L** (I_{478}) increases with the increasing concentration of Al^{3+} and a clear bend of the curve was observed at 1.0 equivalent of added Al^{3+} which prove 1:1 stoichiometry of the $[Al(L)]^+$. Such type of sigmoid curve reflects nature of interaction between the organic probe and Al^{3+} ion. Upon addition of 1-3 μM of Al^{3+} to 10 μM solution of chemosensor, very small change of fluorescence intensity of the probe at wavelength 478 nm has been observed. Upon gradual addition of Al^{3+} from 4-9 μM fluorescence intensity increases from 300-1400 a.u. which indicates strong interaction between Schiff base ligand and Al^{3+}. Maximum increase of fluorescence intensity has been observed upto 10 μM addition of Al^{3+}. This clearly indicates a 1:1 binding between **H_2L** and Al^{3+}. The curve became a plateau with further addition of Al^{3+}, when further increment in fluorescence intensity has not been observed.

Enhancement in fluorescence intensity of **H_2L** in presence of Al^{3+} probably due to elimination of photoinduced electron transfer (PET) in free **H_2L** followed by chelation enhancement effect (CHEF) through the co-ordination of azomethine-N and phenolic-O to metal ion (Scheme 2). Hence, upon complexation a large CHEF effect is observed because of the rigid framework and thereby obstructs the PET process. Thus, upon coordination with Al^{3+} ion, the PET process within the ligand system would become weak by reduction of either the electron-accepting ability of the π-conjugated system of two aromatic rings, >C=N– and azo (-N=N-) groups or the electron-donating ability of the phenoxido oxygen atoms.

View Article Online
DOI: 10.1039/C6RA21217D

Fluorescence intensity of **H_2L** has been examined with various cations (Cd^{2+}, Co^{2+}, Cr^{3+}, Cu^{2+}, Fe^{3+},Hg^{2+}, K^+, Mn^{2+} ,Na^+,Ni^{2+}, Sn^{2+}, Zn^{2+}, Ag^+, Fe^{2+} and Ca^{2+}) using their nitrate salt. (Fig. S13). Fig. S13 shows that only Al^{3+} can induce significant enhancement of fluorescence intensity. Interestingly, upon addition of different metal ions the intensity of the fluorescence either remains unchanged or weakened. In presence of Co^{2+}, Cr^{3+}, Cu^{2+}, K^+, Mn^{2+} ,Na^+,Ni^{2+}, Fe^{2+} and Ca^{2+} metal ions emission intensity remain almost unchanged and in presence of Fe^{3+} Cd^{2+}, Sn^{2+}, Ag^+, Hg^{2+}, and Zn^{2+} metal ions emission intensity slightly increased (Fig. S13). A competition assay of **H_2L** in the presence of Al^{3+} and other metal ions have also been studied and presented in Fig. 5, which prove that fluorescence enhancement due to Al^{3+} nullify the possible interference of other metal ions. Upon addition of different anions viz. $S_2O_3^{2-}$, S^{2-}, SO_3^{2-}, SO_4^{2-}, SCN^-, N_3^-, AsO_4^{3-}, PO_4^{3-}, ClO_4^-, AcO^-, Cl^-, NO_2^-, NO_3^- and SCN^- in HEPES buffer at pH 7.4 (Fig. 6) chemosensor **H_2L** showed no significant fluorescence enhancement. Thus, the probe is an excellent example of fluorescence chemosensor towards Al^{3+} in the presence of different metal ions.

To find out the binding ability of our chemosensor **H_2L** with Al^{3+} ions, binding constant was calculated using Benesi-Hildebrand equation (Equation 1) involving fluorescence titration curve.

$$\frac{F_{max}-F_0}{F_x-F_0} = 1 + \left(\frac{1}{K[C]^n}\right) \qquad (1)$$

Where, F_{max}, F_0 and F_x are fluorescence intensities of **H_2L** in the presence of Al^{3+} at saturation, free **H_2L** and any intermediate Al^{3+} concentration at λ_{max}= 478 nm. K is the dissociation constant of the complex. Concentration of Al^{3+} ions is represented by C and slop n is measured with Hill plot. Then Binding constant (Ka) of the complex has been determined using

View Article Online
DOI: 10.1039/C6RA21217D

the relation, Ka= $1/K_d$. A plot of $\frac{F_{max}-F_0}{F_x-F_0}$ vs $\left(\frac{1}{[M]^1}\right)$ provides the apparent binding constant value as 3.31 x 10^3 M^{-1} (Fig. S14) (n=1.0).[14e] The Job's plot suggests that the ligand **H_2L** forms 1:1 complex with Al^{3+} ions (Fig. S15-16). To determine the binding stoichiometry of **H_2L** and Al^{3+} fluorescence intensity is plotted against different mole fractions of Al^{3+} while volume of solution has remained constant (Fig. S16). Maxima in this plot has been obtained at 0.5 mole fraction, which suggests about 1 : 1 complex formation of **H_2L** and Al^{3+}. The formation of the complex further confirmed from ESI Mass spectroscopy. Mass spectrum of **H_2L** in the presence of Al^{3+} shows peak *m/z* at 575.25 which is corresponding to cationic part of the complex **1** $[Al(L)]^+$ (Fig. S10). The simulated pattern shows well agreement with that of experimental values (Fig. S17). Experimental findings (absorption spectra and fluorescence spectra of Al^{3+} and other cations and various anions with chemosensor **H_2L**) clearly revealed that **H_2L** has strong affinity towards Al^{3+}. Here Al^{3+} acts as strong Lewis acid which can simply binds with two phenoxido oxygen atoms and two imine nitrogen atoms of the Schiff base ligand. Thus the chemosensor acts as a tetradentate N2O2 donor ligand and form a distorted tetrahedral complex with Al^{3+}. Comparable size of the inner-cavity of the chemosensor and Al^{3+} i.e. suitable size and high charge density of Al^{3+} permits strong interaction between **H_2L** and the metal ion.

Fluorescence decay behavior of **H_2L** and complex **1** has been studied. Decay curves have been given in Supplementary Information (Fig. 7). Fluorescence life time of **H_2L** is found to quite low (1.324 ns). Fluorescence life time of **H_2L** in presence of one eq. of Al^{3+}, increases up to 2.058 ns. Quantum yields of **H_2L** and complex **1** are calculated using equation 2 and found to be very low. These have been measured to be 0.00939 and 0.2133, respectively (Table S1). It is to be noted that although quantum yield of the complex is low but it is almost ~22 folds greater compared to free **H_2L**.

View Article Online
DOI: 10.1039/C6RA21217D

$$\Phi_x = \Phi_s \left(\frac{F_x}{F_s}\right)\left(\frac{A_s}{A_x}\right) \quad \ldots\ldots\ldots\ldots\ldots\ldots\ldots\ldots\ldots\ldots\ldots\ldots(2)$$

Where F_x, F_s are the wavelength integrated emission intensities of the samples and reference (here reference is Coumarine); A_s, A_x are the optical densities at their corresponding wavelengths of excitation.

Free ligand upon excitation gives peak at 510 nm. In presence of Al^{3+} there is a slight blue shift ~32 nm of intensity and emission peak observed at 478 nm. Upon gradual addition of Al^{3+} to **H_2L** a steady increase in emission intensity at 478 nm has been observed.

Sensitivity of **H_2L** towards Al^{3+} has been checked by determining limit of detection (LOD) value. The detection limit of the chemosensor was calculated using 3σ method[51] and it is found to be 6.93 x 10^{-9} mol/L.[14e] Low LOD value clearly indicate high sensitivity of **H_2L** towards Al^{3+} ion. In Table S1 some recently published chemosensors for Al^{3+} ion has been reported along with their LOD values.[14a,14e,14g,14i-14o] The reported chemosensor has some advantages over the others while it has some draw backs also. Our probe is synthesized by easy single step Schiff base condensation process. LOD value is significantly low but not the lowest among all.

We also examined fluorescence intensity of **H_2L** in absence and presence of Al^{3+} ion at various pH values. We have maintained the pH range from 3 to 10. The solution concentration of both **H_2L** and Al^{3+} is 10 μM respectively. It has been observed that the chemosensor in free condition exhibit very little fluorescence in the acidic condition (p^H =3 to p^H =7). Fluorescence intensity remains unchanged within this p^H range. Upon increasing pH from 7 to 10 a slight increase in fluorescence intensity has been observed. In presence of Al^{3+}, in acidic condition (p^H =3 to p^H =5) fluorescence intensity of the chemosensor remain unchanged due to protonation of phenolic hydroxyl group of the ligand, therefore nullifying chelation ability with Al^{3+}. Al^{3+} ion

View Article Online
DOI: 10.1039/C6RA21217D

sensing abilities were exhibited by the ligand when pH was increased from 5.0 to 8.0. Thus, **H_2L** exhibited good fluorescence sensing ability towards Al^{3+} ion over a wide range of p^H (Fig. 8). Based on the experimental results we can conclude that our chemosensor can be utilized as a selective fluorescent probe to recognize and distinguish Al^{3+} ion in presence of other metal ions in biological system under physiological condition.

DFT study

Geometry optimization of both **H_2L** and $[Al(L)]^+$ has been performed using DFT/B3LYP method. Mass spectral data analysis has confirmed that the composition of the complex ion is $[Al(L)]^+$. The energy minimized structure of both **H_2L** and $[Al(L)]^+$ are shown in Fig 9. Some selected bond distances and bond angles of the optimized geometries of $[Al(L)]^+$ are listed in Table 3. DFT optimized structure reveals that Al^{3+} is tetra-coordinated and distorted tetrahedral in geometry (Fig. 9) where the chemosensor **H_2L** act as a N2O2 donor center and binds to Al^{3+} through phenolic-O atom and imine-N. Theoretically calculated Al–N(imine) and Al–O(phenolato) distances are around 1.906Å and 1.326Å, respectively and have been comparable with similar structure.[14e] It is interesting to mention that upon complex formation the C(15)–N(3), C(17)–N(4), C(1)–O(1) and C(20)–O(2) bond distances have been significantly elongated compared to free ligand (Table 3). Theoretical calculations show that electron density in both HOMO and LUMO of **H_2L** is mainly distributed on the one part of the aromatic moiety. In metal complex ion i.e. $[Al(L)]^+$ electron density in both HOMO and LUMO is allocated over the entire ligand system. Energy of some selected M.O. of both **H_2L** and $[Al(L)]^+$ are given in Table S3. Mulliken charge distribution shows positive charge on aluminium ion i.e. 1.227343. Mulliken charge distribution of $[Al(L)]^+$ is provided in Table S4.

View Article Online
DOI: 10.1039/C6RA21217D

TDDFT study

For better understanding of electronic transition, TDDFT calculations were performed using B3LYP/CPCM method using same basis sets in acetonitrile. The calculated electronic transitions are given in Table 4. **H_2L** shows intense absorption band for ligand based n-π and π–π* transitions around 290 nm and 388 nm respectively. The band at 290 nm is due to the contribution of HOMO−4→LUMO+1and HOMO→LUMO+2 transitions, whereas the band at 388 nm is due to the contribution of HOMO−1→LUMO, HOMO−1→LUMO+1 and HOMO→LUMO transitions. For the L–Al species the intense absorption band around 375 nm corresponding to HOMO→LUMO+1, HOMO→LUMO+2, HOMO→LUMO+3 and HOMO−2 →LUMO transitions (Fig. 10). The spectra calculated for the ligand and L–Al species were found to be compatible with those obtained experimentally. It is important to mention that in case of $[Al (L)]^+$ species all transitions are ligand based.

In order to have better understanding of the emission spectrum we have optimized the triplet state (T1) of both ligand (**H_2L**) and ($[Al(L)]^+$) using same basis set. The emission wavelength obtained from the computation is very much comparable with that of experimental data. The data i.e. emission wavelength, emission energies and the nature of the transition obtained from the computation are given in Table 5. The emission band of the chemosensor (**H_2L**) at 510 nm was theoretically obtained at 509.84 nm with major key transitions of HOMO(α)→LUMO(α)+1(58%), HOMO(α)→LUMO(α)+2(10%) and HOMO(β)−1→LUMO(β) (11%) respectively. Whereas for the $[Al(L)]^+$ the emission band at 478 nm was theoretically obtained at 476.93 with major key transitions viz. HOMO(β)→LUMO(β)+2(22%) and HOMO(α) -1 →LUMO(α) (66%) respectively.

View Article Online
DOI: 10.1039/C6RA21217D

NMR studies

Firstly, the chemosensor was well characterized in $CDCl_3$ solvent. In $CDCl_3$, imine proton appeared at 8.43 ppm. Aromatic, aliphatic and methoxy protons appeared at 7.42-7.90 ppm, 3.82-3.84 ppm, 2.25 ppm and 4.01 ppm respectively. Then, we have performed ^{1}H NMR studies of both free **H_2L** and **H_2L**+Al^{3+} in 1:1 molar ratio in DMSO-d_6 solvent (Fig. 11). The free chemosensor (**H_2L**) exhibit clear peaks for different protons. Imine proton appears at 8.66 ppm. All aromatic protons appear as multiplate at around 7.74-7.30 ppm. Aliphatic protons appear as multiplate at 3.74 and 2.06 ppm respectively. –OCH_3 protons appear around 3.74 ppm. In NMR spectrum signal of aliphatic one –CH_2 got merged with that the signal of –OCH_3. Unfortunately we could not identify signal for phenolic OH proton due to extensive hydrogen bonding with solvent molecules. Upon addition of Al^{3+} to the chemosensor peak positions of different protons have changed significantly. Imine protons have shifted notably from 8.66 ppm to 9.24 ppm indicating coordination of imine nitrogen with aluminium ion. In case of aromatic and aliphatic protons broadening and overlapping of signals observed. Therefore, formation of complex **1** in the presence of Al^{3+} is strongly evidenced from the NMR spectral studies.

Molecular logic gates

The property of this chemosensor encourages us to construct a molecular logic gate with two binary inputs. The two inputs are Al^{3+} and Na_2EDTA where the output is monitored as change in fluorescence emission spectrum at 478 nm. In absence of both of the inputs there is no significant change in emission band which implies that the gate is 'OFF'. On addition of Na_2EDTA to the chemosensor there is no significant changes, rather the emission band remained

View Article Online
DOI: 10.1039/C6RA21217D

unchanged. So, in presence of Na_2EDTA the output was considered to be zero. On the other hand, upon addition of Al^{3+} ion solution alone to the chemosensor shows significant enhancement of the fluorescence intensity at 478 nm and now the output signal is 1 i.e. the gate is 'ON'. However in presence of both of the inputs the fluorescence intensity is significantly quenched and the output is zero implying that the gate is 'OFF' again. These studies suggest that this molecular gate is acting as INHIBIT (INH) logic gate where the inputs and output are Al^{3+}, Na_2EDTA and change in fluorescence intensity at 478 nm, respectively. It is basically an 'AND' gate which has one of its inputs is negated. The input which is negated, acts to inhibit the gate. We can say that the gate will behave like an 'AND' gate only when the negated input is set at a logic level '0'. Here the negated input is Na_2EDTA. The respective truth table and pictorial diagram of the INH logic gate is depicted in Fig.12 and Table 6.

Conclusion

In summary, an azo based low cost, simple, easy to prepare, chemosensor **H_2L** has been successfully prepared which is capable of recognizing Al^{3+} ion in presence of large number of other metal ions in HEPES buffer solution (1:100 v/v, HEPES buffer at pH 7.4) at 25 °C. The chemosensor has been structurally characterized. Fluorescence intensity of the probe has enhanced by ~61 fold in presence of Al^{3+}. The low detection limit of **H_2L** for Al^{3+} (6.93 nM) suggests that the chemosensor could be a good choice for efficient monitoring of the Al^{3+} in real samples. **H_2L** forms 1:1 complex with Al^{3+} which has been established by 1H NMR, MS studies and further supported by DFT calculations. **H_2L** exhibited good fluorescence sensing ability towards Al^{3+} ion over a wide range of p^H, therefore, **H_2L** could be successfully applied to living cells for detecting Al^{3+}. We also establish Molecular logic gates (INH) based on two inputs (Al^{3+}

View Article Online
DOI: 10.1039/C6RA21217D

and EDTA)and one Output. Thus, this probe could be considered as a potential candidate for sensing Al^{3+} in less organic solvents.

Acknowledgments

A. S. gratefully acknowledges the financial support of this work by the DST, India (Sanction No. SB/FT/CS-102/2014, dated- 18.07.2015). The authors are thankful to Prof. Mahammad Ali and Mr. Pravat Ghorai, Department of Chemistry, Jadavpur University, India for their scientific suggestions.The authors also acknowledge the use of the DST-funded National Single Crystal X-ray Diffraction Facility at the Department of Chemistry, Jadavpur University, Kolkata-700032, India for X-ray crystallographic studies.

Appendix A. Supplementary data

CCDC 1478332-1478333 contain the supplementary crystallographic data for azoaldehyde and **H_2L**. This data can be obtained free of charge via http://www.ccdc.cam.ac.uk/conts/retrieving.html, or from the Cambridge Crystallographic Data Centre, 12 Union Road, Cambridge CB2 1EZ, UK; fax: (+44) 1223-336-033; or email:deposit@ccdc.cam.ac.uk.

Notes and References

[a]*Department of Chemistry, Jadavpur University, Kolkata- 700032, India.*

E-mail: asaha@chemistry.jdvu.ac.in; amritasahachemju@gmail.com; Tel. +91-33-24572941

[b]*TEMA−NRD, Mechanical Engineering Department, University of Aveiro, 3810-193 Aveiro, Portugal*

View Article Online
DOI: 10.1039/C6RA21217D

References

1 M. G. Sont, S. M. White, W. G. Flamm and G. A. Burdock, *Regul. Toxicol. Pharmacol*., 2001, **33**, 66-79.

2(a) D. R. Crapper, S. S. Krishnan and A. J. Dalton, *Science*, 1973, **180**, 511-513; (b) D. P. Perl and A. R. Brody, *Science*, 1980, **208**, 297-299; (c) E. House, J. Collingwood, A. Khan, O. Korchazkina, G. Berthon and C. J. Exley, *J. Alzheimers Dis*., 2004, **6**, 291-301.

3 G.C. Woodson, *Bone*, 1998, **22,** 695-698.

4 P.D. Darbre, *J. Inorg. Biochem*., 2005, **99**,1912-1919.

5 R. W. Gensemer and R. C. Playle, *Crit. Rev. Environ. Sci. Technol*., 1999, **29**, 315-450.

6(a) A. Budimir, *Acta Pharm*., 2011, **61**, 1; (b) P. Nayak, *Environ. Res.*, 2002, **89**, 101-115; (c) P. Zatta, *Coord. Chem. Rev*., 2002, **228**, 271-284.

7 (a) J. Barcelo and C. Poschenrieder, *Environ. Exp. Bot*., 2002, **48**, 75-92; (b) B. Valeur and I. Leray, *Coord. Chem. Rev*., 2000, **205**, 3-40; (c) Z. Krejpcio and R. W. P. J. Wojciak, *Environ. Stud.*, 2002, **11**, 251-254.

8 K. Soroka, R. S. Vithanage, D. A. Phillips, B. Walker and P. K. Dasgupta, *Anal. Chem*., 1987, **59**, 629-636.

9 A. Zioła-Frankowska, M. Frankowski and J. Siepak, *Talanta*, 2009, **79**, 623-630.

10 F. Zheng and B. Hu, *Spectrochim. Acta, Part B*, 2008, **63**, 9-10.

11 F. Thomas, A. Maslon, J. Y. Bottero, J. Rouiller, F. Montlgny and F. Genevrlere, *Environ. Sci. Technol.*, 1993, **27**, 2511-2516.

View Article Online
DOI: 10.1039/C6RA21217D

12 Y. H. Ma, R. Yuan, Y. Q. Chai and X. L. Liu, *Mater. Sci. Eng*., 2010, **30**, 209-224.

13 K. Soroka, R. S.Vithanage, D. A. Phillips, B. Walker and P. K. Dasgupta, *Anal. Chem*., 1987, **59**, 629-636.

14 (a) L. Wang, W. Qin, X. Tang, W. Dou, W. Liu, Q. Teng and X. Yao, *Org. Biomol.Chem*., 2010, **8**, 3751-3157; (b) K. K. Upadhyay and A. Kumar, *Org. Biomol. Chem*., 2010, **8**, 4892-4897; (c) F. K. Hau, X. He, W. H. Lam and V. W. Yam, *Chem. Commun*., 2011, **47**, 8778-8780; (d) A. Sahana, A. Banerjee, S. Das, S. Lohar, D. Karak, B. Sarkar, S. K. Mukhopadhyay, A. K. Mukherjee and D. Das, *Org. Biomol.Chem*., 2011, **9**, 5523-5529; (e) A. Banerjee, A. Sahana, S. Das, S. Lohar, S. Guha, B. Sarkar, S. K. Mukhopadhyay, A. K. Mukherjee and D. Das, *Analyst*, 2012, **137**, 2166-2175; (f) D. Karak, S. Lohar, A. Sahana, S. Guha, A. Banerjee and D. Das, *Anal Methods*, 2012, **4**, 1906-1908; (g) D. Karak, S. Lohar, A. Banerjee, A. Sahana, I. Hauli, S. K. Mukhopadhyay, J. S. Matalobos and D. Das, *RSC Adv*., 2012, **2**, 12447-12454; (h) A. Sahana, A. Banerjee, S. Lohar, S. Das, I. Hauli, S. K. Mukhopadhyay, J. S. Matalobos and D. Das, *Inorg. Chim. Acta*, 2012, **12**, 12-13.(i) A. Sahana, A. Banerjee, S. Lohar, B. Sarkar, S.K. Mukhopadhyay and D. Das, *Inorg. Chem.*, 2013, 52, 3627−3633 and references cited herein; (j) D. Maity and T. Govindaraju, *Inorg. Chem.,* 2010, 49, 7229–7231; (k) J. Ma, W. Shi, L. Feng, Y. Chen, K. Fan, Y. Hao, Y. Hui A and Z. Xie, *RSC Advances*, 2016, 2016, **6**, 28034-28037; (l) B. Sen, M. Mukherjee, S. Banerjee, S. Pala and P. Chattopadhyay, *Dalton trans*., 2015, **44**, 8708-8717; (m) J. Kumar, M. J. Sarma, P. Phukan and D. K. Das, *Dalton Trans*., 2015, **44**, 4576-4581; (n) C. Kar, S. Samanta, S. Goswami, A. Ramesh and G. Das, *Dalton trans*., 2015, **44**, 4123-4132; (o) S. Goswami, K. Aich, S. Das, A. Kumar Das, D. Sarkar, S. Panja, T.K. Mondal and S. Mukhopadhyay, *Chem. Commun.,* 2013, **49**, 10739-10741; (p) A. Roy, S. Dey and Partha Roy, *Sensors and Actuators B,* 2016,**B 237,** 628–642 and references cited herein.

View Article Online
DOI: 10.1039/C6RA21217D

498

499 15 (a) Z. Xu, Y. Xiao, X. Qian, J. Cui and D. Cui, *Org. Lett*., 2005, **7**, 889. (b) J. B. Wang, X. F.

500 Qian and J. N. Cui, *J. Org. Chem*., 2006, **71**, 4308-4311.

501 16 (a) T. Gunnlaugsson, A. P. Davis, J. E. O'Brien and M. Glynn, *Org. Lett*., 2002, **4**, 2449-

502 2452; (b) D. H. Vance and A. W. Czarnik, *J. Am. Chem. Soc*., 1994, **116**, 9397-9398; (c) S. K.

503 Kim and J. Yoon, *Chem. Commun*., 2002, 770-771.

504 17 (a) N. C. Lim, J. V. Schuster, M. C. Porto, M. A. Tanudra, L. Yao, H. C. Freake and C.

505 Bruckner, *Inorg. Chem*., 2005, **44**, 2018-2030; (b) S. Guha, S. Lohar, A. Banerjee, A. Sahana, A.

506 Chaterjee, S. K. Mukherjee, J. S. Matalobos and D. Das, *Talanta*, 2012, **91**, 18-25; (c) S. Das, A.

507 Sahana, A. Banerjee, S. Lohar, S. Guha, J. S. Matalobos and D. Das, *Anal. Methods*, 2012, **4**,

508 2254-2258.

509 18 (a) P. D. Beer, *Acc. Chem. Res*., 1998, **31**, 71-80; (b) M. J. Kim, R. Konduri, H. Ye, F. M.

510 MacDonnell, F. Puntoriero, S. Serroni, S. Campagna, T. Holder, G. Kinsel and K. Rajeshwar,

511 *Inorg. Chem*., 2002, **41**, 2471-2476.

512 19 (a) S. Nishizawa, Y. Kato and N. Teramae, *J. Am. Chem. Soc*., 1999, **121**, 9463-9464; (b) J.-

513 S. Wu, J.-H. Zhou, P.-F. Wang, X.-H. Zhang and S.- K. Wu, *Org. Lett*., 2005, **7**, 2133-2136; (c)

514 B. Schazmann, N. Alhashimy and D. Diamond, *J. Am. Chem. Soc*., 2006, **128**, 8607-8614; (d) A.

515 Banerjee, A. Sahana, S. Guha, S. Lohar, I. Hauli, S. K. Mukhopadhyay, J. S. Matalobos and D.

516 Das, *Inorg. Chem*., 2012, **51**, 5699-5704; (e) A. Sahana, A. Banerjee, S. Lohar, S. Guha, S. Das,

517 S. K. Mukhopadhyay and D. Das, *Analyst*, 2012, **137**, 3910-3913.

518 20 J.-S. Wu, W.-M. Liu, X.-Q. Zhuang, F. Wang, P.-F. Wang, S.-L. Tao, X.-H. Zhang, S.-K. Wu

519 and S.-T. Lee, *Org. Lett*., 2007, **9**, 33-36.

View Article Online
DOI: 10.1039/C6RA21217D

21 (a) A. Sahana, A. Banerjee, S. Guha, S. Lohar, A. Chattopadhyay, S. K. Mukhopadhyay and D. Das, *Analyst*, 2012, **137**, 1544-1546; (b) S. Lohar, A. Sahana, A. Banerjee, A. Banik, S. K. Mukhopadhyay, J. S. Matalobos and D. Das, *Anal. Chem*., 2013, **85**, 1778-1783; (c) S. Das, S. Guha, A. Banerjee, S. Lohar, A. Sahana and D. Das, *Org. Biomol. Chem*., 2011, **9**, 7097-7104.

22 X. Peng, Y. Wu, J. Fan, M. Tian and K. Han, *J. Org. Chem*., 2005, **70**, 10524-10531.

23 (a) J. M. Serin, D. W. Brousmiche and J. M. J. Frechet, *J. Am. Chem. Soc*., 2002, **124**, 11848-11849; (b) A. E. Albers, V. S. Okreglak and C. J. Chang, *J. Am. Chem. Soc.,* 2006, **128**, 9640-9641; (c) S. H. Lee, S. K. Kim, J. H. Bok, S. H. Lee, J. Yoon, K. Lee and J. S. Kim, *Tetrahedron Lett.,* 2005, **46**, 8163-8167; (d) W. R. Dichtel, J. M. Serin, C. Edder, J. M. J. Frechet, M. Matuszewski, L.-S. Tan, T. Y. Ohulchanskyy and P. N. Prasad, *J. Am. Chem. Soc*., 2004, **126**, 5380-5381; (e) M. Suresh, S. Mishra, S. K. Mishra, E. Suresh, A. K. Mandal, A. Shrivastav, A. Das, *Org. Lett*., 2009, **11**, 2740-2743; (f) P.Mahato, S.Saha, E.Suresh, R. D.Liddo, P. P. Parnigotto, M. T. Conconi, M. K. Kesharwani, B. Ganguly and A. Das, *Inorg. Chem*., 2012, **51**, 1769-1777; (g) K. Sreenath, J. Allen, R. M. W. Davidsonand L. Zhu, *Chem. Commun*., 2011, **47**, 11730-11732;(h) R. J.Wandell, A. H.Younes and L. Zhu, *New J. Chem*.,2010, **34**, 2176-2182; (i) S. Lohar, A. Banerjee, A. Sahana, A. Banik, S. K. Mukhopadhyay and D. Das, *Anal Methods,* 2013, **5**, 442-445.

24 (a) A. Natansohn and P. Rochon, *Chem. Rev*., 2002, **102**, 4139-4176; (b) A. S. Matharu, S. Jeeva and P. S. Ramanujam, *Chem. Soc. Rev.*, 2007, **36**, 1868-1880; (c) T. Ikeda, *J. Mater. Chem*., 2003, **13**, 2037-2057; (d) S. Kubo, Z. Z. Gu, K. Takahashi, A. Fujishima, H. Segawa and O. Sato, *J. Am. Chem. Soc.*, 2004, **126**, 8314-8319; (e) C. Dohno, S. N. Uno and K. Nakatani, *J. Am. Chem. Soc*., 2007, **129**, 11898-11899; (f) N. Kano, F. Komatsu, M. Yamamura and T.

View Article Online
DOI: 10.1039/C6RA21217D

542 Kawashima, *J. Am. Chem. Soc*., 2006, **128**, 7097-7106; (g) A. Archut, F. Vogtle, L. De Cola, G.
543 C. Azzellini, V. Balzani, P. S. Ramanujam and R. H. Berg, *Chem.–Eur. J*., 1998, **4**, 699-706.
544 25 A. Abbotto, L. Beverina, N. Manfredi, G. A. Pagani, G. Archetti, H. G. Kuball, C.
545 Wittenburg, J. Heck and J. Holtmann, *Chem.–Eur. J*., 2009, **15**, 6175-6185.
546 26 S. Kawata and Y. Kawata, *Chem. Rev*., 2000, **100**, 1777-1788.
547 27 Y. T. Li, C. L. Chen, Y. Y. Hsu, H. C. Hsu, Y. Chi, B. S. Chen, W. H. Liu, C. H. Lai, T. Y.
548 Lin and P. T. Chou, *Tetrahedron*, 2010, **66**, 4223-4229.
549 28 X. C. Chen, T. Tao, Y. Ge Wang, Y. X. Peng, W. Huang and H. F. Qian, *Dalton Trans.,*
550 2012, **41**, 11107-11115.
551 29 (a) M. E. Moustafa, M. S. McCready and R. J. Puddephatt, *Organometallics*, 2012, **31**, 6262-
552 6269; (b) M. E. Moustafa, M. S. McCready and R. J. Puddephatt, *Organometallics*, 2013, **32**,
553 2552-2557; (c) G. C. Hampson and M. Robertson, *J. Chem. Soc.,* 1941, 409-413.
554 30 A. Kumar, A. Kumar and D.S. Pandey, *Dalton Trans*., 2016, **45**, 8475-8484.
555 31 G.M. Sheldrick, SAINT, Version 6.02, SADABS, Version 2.03, Bruker AXS Inc., Madison,
556 Wisconsin, 2002.
557 32 G.M. Sheldrick, SADABS: Software for Empirical Absorption Correction, University of
558 Gottingen, Institute fur Anorganische Chemieder Universitat, Gottingen, Germany, 1999-2003.
559 33 G. M. Sheldrick, *Acta Cryst*., 2008, **A64**, 112-122.
560 34 M.J. Frisch, G.W. Trucks, H.B. Schlegel, G.E. Scuseria, M.A. Robb, J.R. Cheeseman, G.
561 Scalmani, V. Barone, B. Mennucci, G.A. Petersson, H. Nakatsuji, M. Caricato, X. Li, H.P.
562 Hratchian, A.F. Izmaylov, J. Bloino, G. Zheng, J.L. Sonnenberg, M. Hada, M. Ehara, K. Toyota,
563 R. Fukuda, J. Hasegawa, M. Ishida, T. Nakajima, Y. Honda, O. Kitao, H. Nakai, T. Vreven, J.A.
564 Montgomery Jr. J.E. Peralta, F. Ogliaro, M. Bearpark, J.J. Heyd, E. Brothers, K.N. Kudin, V.N.

View Article Online
DOI: 10.1039/C6RA21217D

565 Staroverov, R. Kobayashi, J. Normand, K. Raghavachari, A. Rendell, J.C. Burant, S.S. Iyengar,
566 J. Tomasi, M. Cossi, N. Rega, J.M. Millam, M. Klene, J.E. Knox, J.B. Cross, V. Bakken, C.
567 Adamo, J. Jaramillo, R. Gomperts, R.E. Stratmann, O. Yazyev, A.J. Austin, R. Cammi, C.
568 Pomelli, J.W. Ochterski, R.L. Martin, K. Morokuma, V.G. Zakrzewski, G.A. Voth, P. Salvador,
569 J.J. Dannenberg, S. Dapprich, A.D. Daniels, Ö. Farkas, J.B. Foresman, J.V. Ortiz, J. Cioslowski,
570 D.J. Fox,GAUSSIAN09, Revision D.01, Gaussian Inc. Wallingford, CT, 2009.

571 35 A. D. Becke, *J. Chem. Phys*., 1993, **98**, 5648-5652.

572 36 C. Lee, W. Yang and R.G. Parr, *Phys. Rev*., 1988, **B 37**, 785-789.

573 37 P.J. Hay and W.R. Wadt, *J. Chem. Phys.,* 1985, **82**, 270-283.

574 38 W.R. Wadt and P.J. Hay, *J. Chem. Phys.,* 1985, **82**, 284-298.

575 39 P.J. Hay and W.R. Wadt, *J. Chem. Phys.,* 1985, **82**, 299-310.

576 40 G.A. Petersson, A. Bennett, T.G. Tensfeldt, M.A. Al-Laham, W.A. Shirley and J. Mantzaris,
577 *J. Chem. Phys.,* 1988, **89**, 2193-2218.

578 41 G.A. Petersson and M.A. Al-Laham, *J. Chem. Phys.,* 1991, **94**, 6081-6090.

579 42 R. Bauernschmitt and R. Ahlrichs, *Chem. Phys. Lett.,* 1996,**256**, 454-464.

580 43R. E. Stratmann, G. E. Scuseria and M. J. Frisch, *J. Chem. Phys.,* 1998, **109**, 8218-8224.

581 44 M.E. Casida, C. Jamorski, K.C. Casida and D.R. Salahub, *J. Chem. Phys.,* 1998, **108**, 4439-
582 4449.

583 45 V. Barone and M. Cossi, *J. Phys. Chem. A,* 1998, **102**, 1995-2001.

584 46 M. Cossi and V. Barone, *J. Chem. Phys*., 2001, **115**, 4708-4717.

View Article Online
DOI: 10.1039/C6RA21217D

47 M. Cossi, N. Rega, G. Scalmani and V. Barone, *J. Comput.Chem*., 2003, **24**, 669-681.

48 N.M. O'Boyle, A.L. Tenderholt and K.M. Langner, *J. Comput. Chem*., 2008, **29**, 839-845.

49 M. T. Wheeler and F. Walmsley, *ThermochimicaActu*, 1986, **108**, 325-336.

50 G. Ozkan , M. Kose , H. Zengin , V. McKee and M. Kurtoglu, *Spectrochimica Acta Part A: Molecular and Biomolecular Spectroscopy,* 2015, **150**, 966-972.

51A. B. Pradhan, S. K. Mandal , S. Banerjee , A. Mukherjee , S. Das, A.R.K. Bukhsh and A. Saha, *Polyhedron*, 2015, **94**, 75-82.

View Article Online
DOI: 10.1039/C6RA21217D

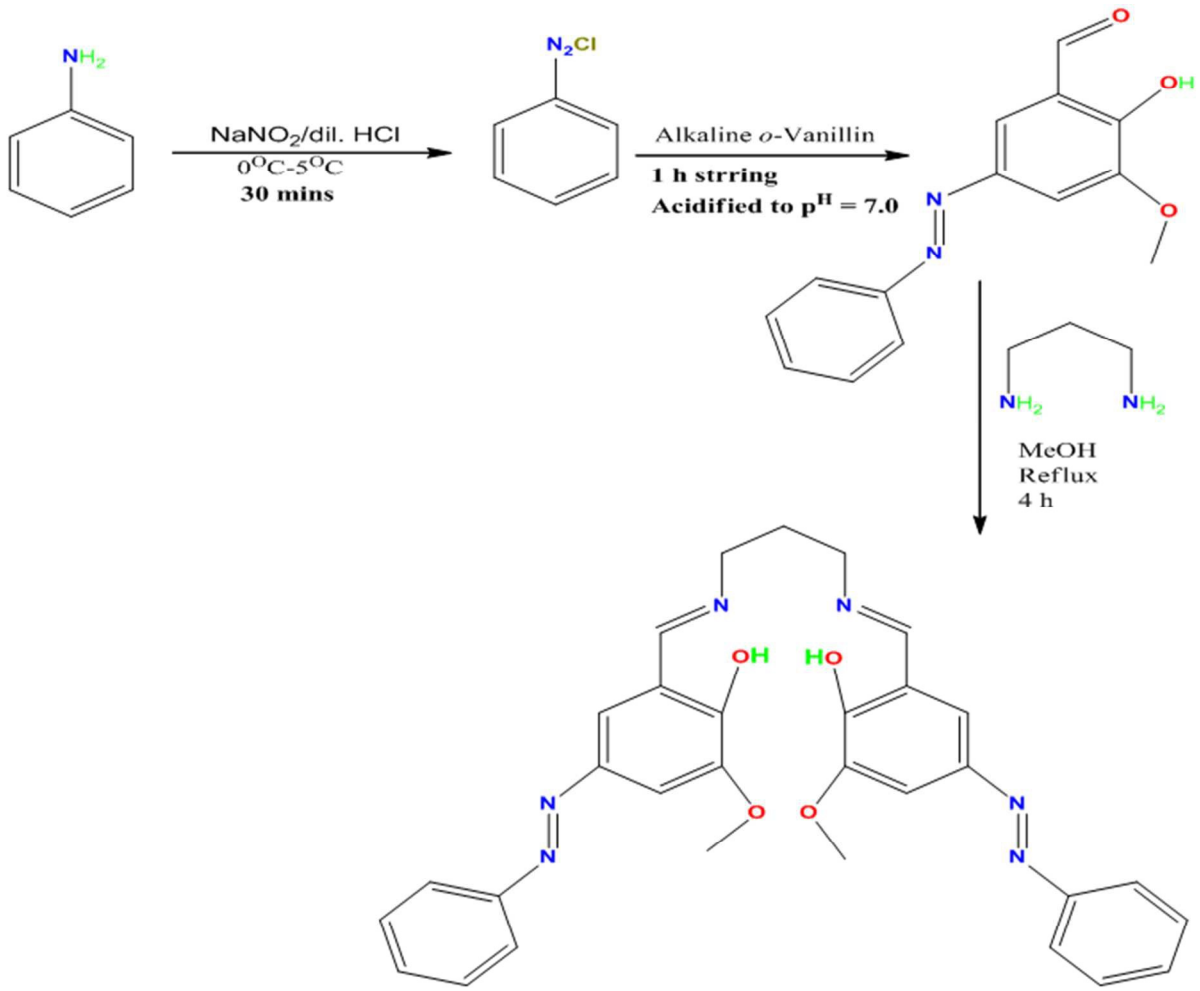

Scheme 1.The route to the syntheses of **H_2L**.

View Article Online
DOI: 10.1039/C6RA21217D

.

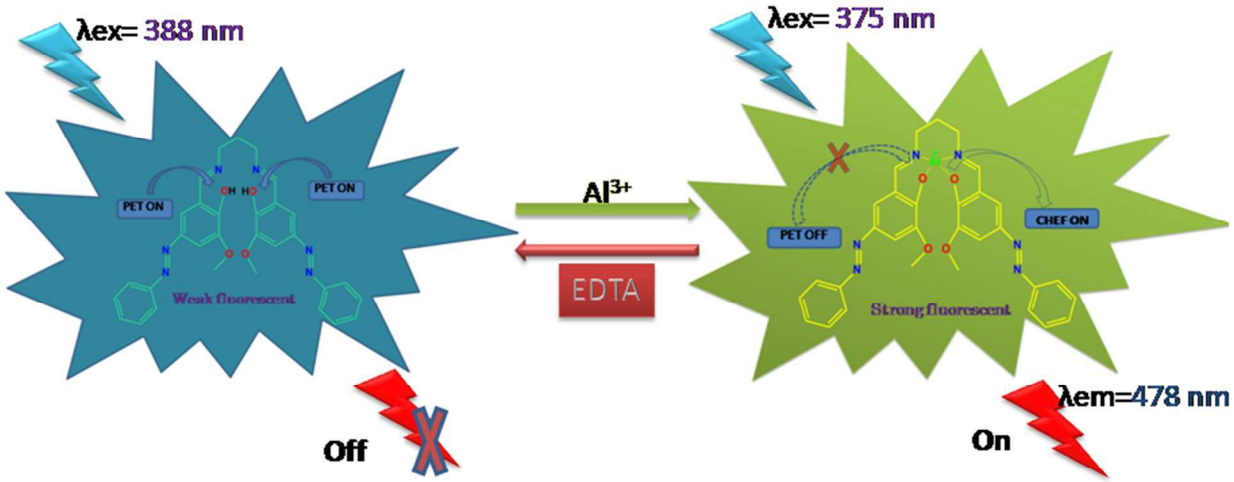

Scheme 2. Schematic diagram for photoinduced electron transfer (PET) in free $\mathbf{H_2L}$ and chelation enhancement effect (CHEF) in $[Al(L)]^+$.

View Article Online
DOI: 10.1039/C6RA21217D

633

634 Table 1. Crystal parameters and selected refinement details for **H_2L.**

Compound	Azoaldehyde	**H_2L**
Empirical formula	$C_{14}H_{12}N_2O_3$	$C_{31}H_{28}N_6O_4$
Formula weight	256.26	548.59
Temperature (K)	155(2)	150(2)
Crystal system	Monoclinic	Triclinic
Space group	CC	
a (Å)	10.7683(4)	8.648(2)
b (Å)	13.4401(5)	11.051(3)
c (Å)	8.4892(3)	13.816(4)
α(°)	90.00	91.833(9)
β(°)	93.755(2)	97.710(9)
γ(°)	90.00	92.902(8)
Volume (Å^3)	1225.98(8)	1305.8(6)
Z	4	2
D_{calc} (g cm^{-3})	1.388	1.395

View Article Online
DOI: 10.1039/C6RA21217D

Absorption coefficient (mm^{-1})	0.100	0.095
F(000)	536	576
θ Range for data collection (°)	2.43-26.40	2.326-23.559
Reflections collected	4910	12084
Independent reflections / R_{int}	2204/0.0313	3806/ 0.0726
Observed reflections [I>2σ(I)]	1980	2308
Data / restraints / parameters	2204/2/175	3806/0/373
Goodness-of-fit on F^2	1.029	1.752
Final indices[I>2σ(I)]	R1= 0.0331 wR2 = 0.0812	R1= 0.1611 wR2 = 0.4280
R indices (all data)	R1= 0.0378 wR2 = 0.0842	R1= 0.2089 wR2 = 0.4619
Largest diff. peak / hole (e $Å^{-3}$)	0.150/-0.120	0.968/-0.620

635

636

637

638

View Article Online
DOI: 10.1039/C6RA21217D

Table 2. Selected bond lengths (Å) and bond angles (°) for **Azoaldehyde** and **H_2L**

Azoaldehyde			**H_2L**		
	X-ray	Calculated		X-ray	Calculated
C3-O2	1.340	1.3450	N1-N2	1.22(1)	1.2645
C8-O1	1.224	1.2264	N5-N6	1.267(9)	1.2647
N1-N2	1.252	1.2611	C15-N3	1.29(1)	1.2853
C2-O3	1.362	1.3631	C17-N4	1.28(1)	1.2845
			C15-C16-C17	114.4(7)	115.79
			C1-O1	1.259	1.275
			C2-O2	1.286	1.297

View Article Online
DOI: 10.1039/C6RA21217D

Table 3. Selected bond lengths (Å) and bond angles (°) of DFT optimized structure of $[Al(L)]^+$.

(B3LYP/6-31+G(d) basis set)

	Calculated		Calculated		Calculated
N1-N2	1.26019	C1-O1	1.32767	Al-O1	1.7584
N5-N6	1.26320	C2-O2	1.32668	Al-O2	1.7553
C15-N3	1.31355	Al-N3	1.90639		
C17-N4	1.31661	Al-N4	1.92372		
C15-C16-C17	115.79	C15-C16-C17	116.50435		

View Article Online
DOI: 10.1039/C6RA21217D

Table 4. Electronic transition calculated by TDDFT using B3LYP/CPCM method in Acetonitrile solvent of Ligand ($\mathbf{H_2L}$) and $\mathbf{[Al(L)]^+}$.

	$E_{excitation}$ (ev)	$\lambda_{excitation}$ (nm)	Osc. Strength (f)	Key transition	Character
Ligand ($\mathbf{H_2L}$)	3.60	344.43	0.1608	HOMO-4→LUMO+1(42%)	π (L)→ π*(L)
	3.57	346.63	0.0469	HOMO→LUMO+2 (29%)	π (L) →π*(L)
	3.19	388.28	0.902	HOMO-1→LUMO (56%)	π (L)→ π*(L)
	3.14	394.53	0.6101	HOMO-1→LUMO+1(48%)	π (L)→ π*(L)
	3.019	410.64	0.0149	HOMO→LUMO (71%)	π (L) →π*(L)
$\mathbf{[Al(L)]^+}$	3.17	390.79	0.2576	HOMO-1→LUMO+1(86%)	π (L)→ π*(L)
	3.15	393.75	0.0254	HOMO→LUMO+2 (82%)	π (L)→ π*(L)
	3.02	411.01	0.0011	HOMO-1→LUMO (86%)	π (L) →π*(L)
	2.95	419.85	0.6153	HOMO→LUMO (89%)	π (L)→ π*(L)

View Article Online
DOI: 10.1039/C6RA21217D

676 Table 5. Emission spectrum calculated by TDDFT using B3LYP basis set for Ligand (**H_2L**) and

677 $[Al(L)]^+$.

	$E_{excitation}$ (ev)	$\lambda_{emission}$(nm)	Excited State	Osc. Strength (f)	Key transition
Ligand (**H_2L**)	2.43	509.84	5	0.0116	HOMO(α)→LUMO(α)+1(58%) HOMO(β)-1→LUMO(β) (11%) HOMO(α)→LUMO(α)+2 (10%)
$[Al(L)]^+$	2.17	476.93	8	0.2476	HOMO(α)-1→LUMO(α)(66%) HOMO(β)→LUMO(β) +2 (22%)

678

679

680

681

682

683

684

685

686

687

View Article Online
DOI: 10.1039/C6RA21217D

Table 6.Truth Table

IN1 (Al^{3+})	IN2 (EDTA)	Output (Emission at 478 nm)
0	0	0
0	1	0
1	0	1
1	1	0

View Article Online
DOI: 10.1039/C6RA21217D

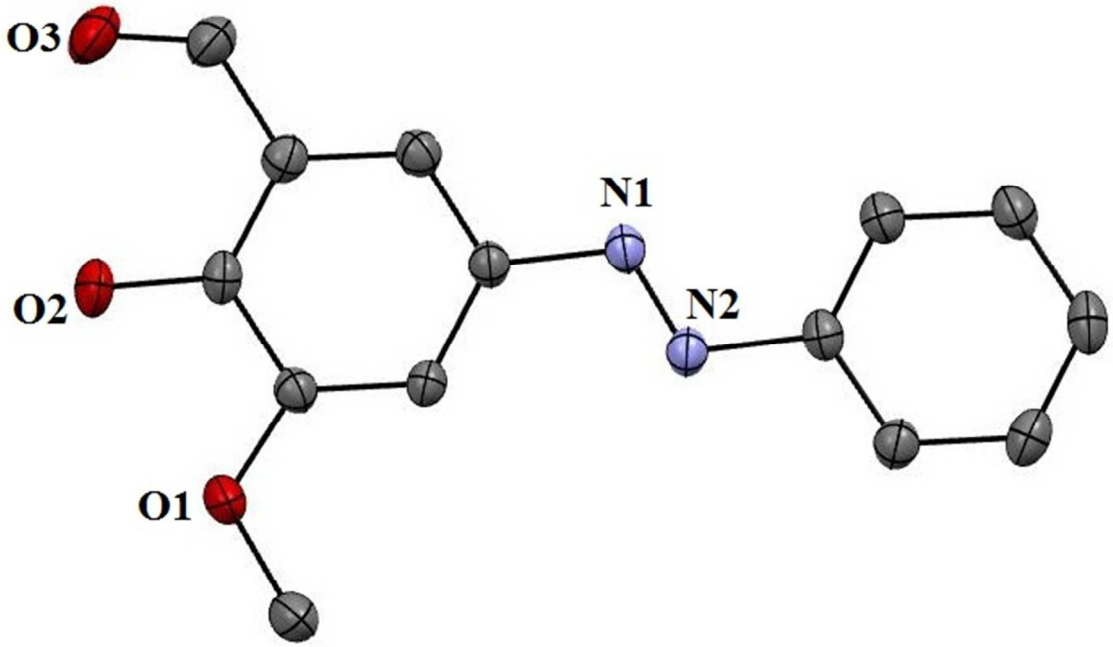

Fig. 1. Ortep view of azoaldehyde. Atoms are shown as 30% thermal ellipsoids. H atoms are omitted for clarity.

View Article Online
DOI: 10.1039/C6RA21217D

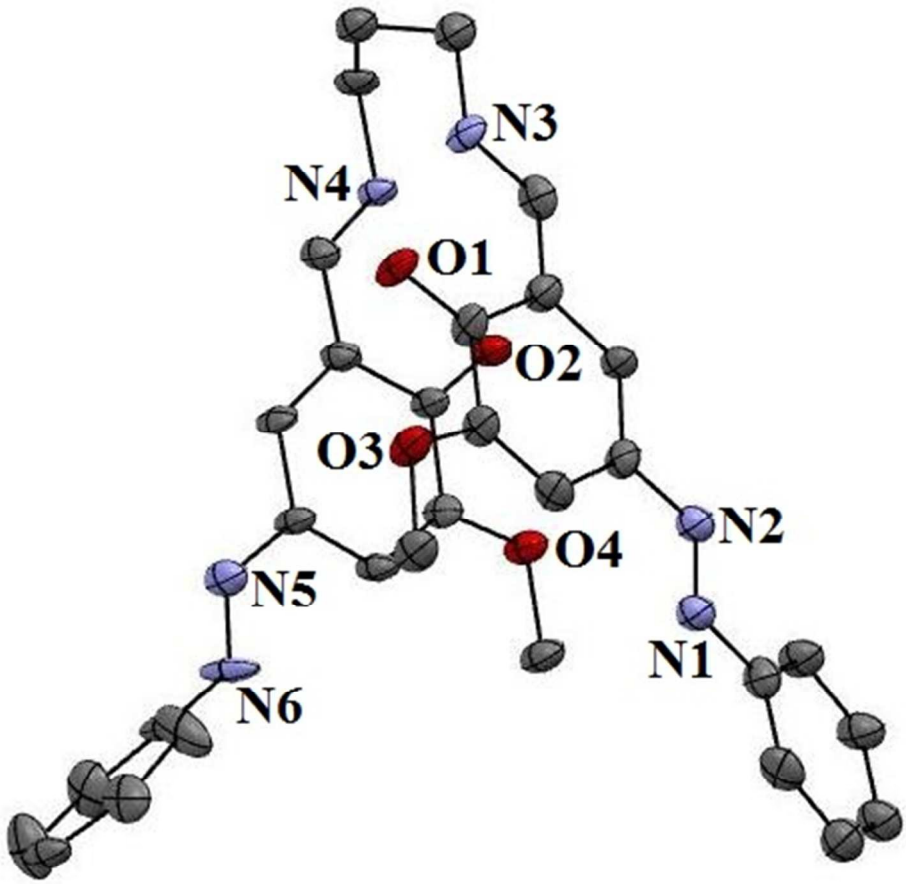

Fig. 2. Ortep view of the ligand (**H_2L**). Atoms are shown as 30% thermal ellipsoids. H atoms are omitted for clarity.

View Article Online
DOI: 10.1039/C6RA21217D

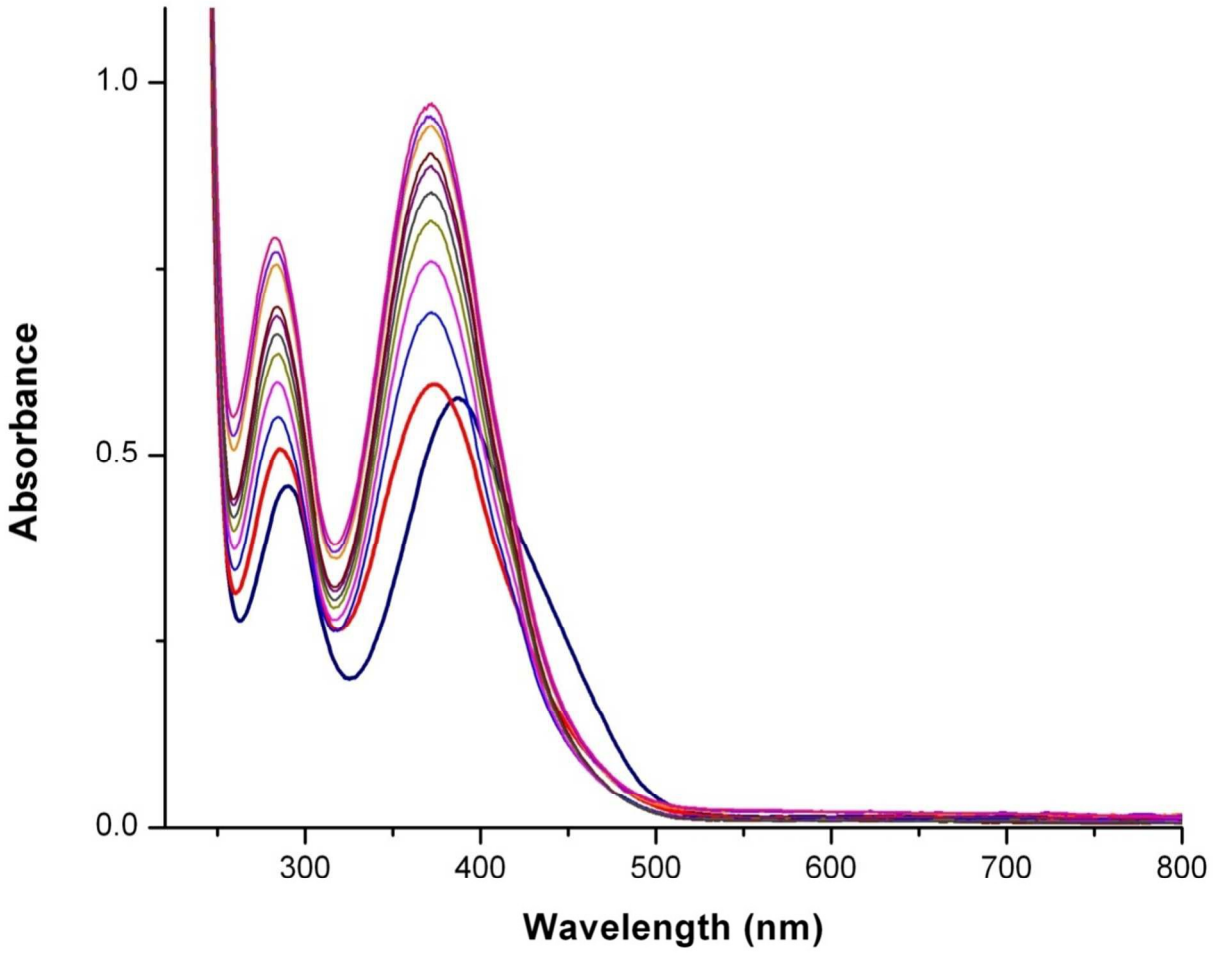

Fig. 3. Absorption titration of **H_2L** (10 μM) with gradual addition of Al^{3+}, 0-10 μM in MeCN/ HEPES buffer at p^H 7.4.

View Article Online
DOI: 10.1039/C6RA21217D

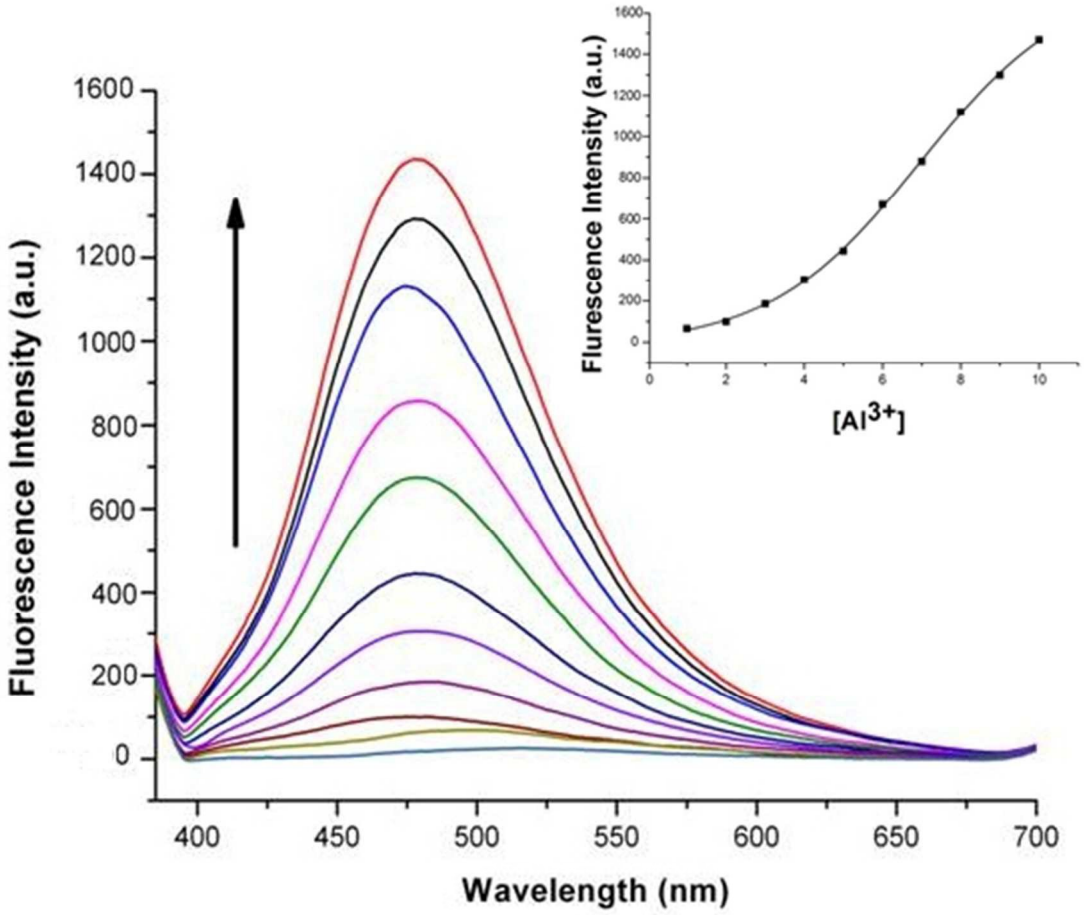

Fig. 4. Fluorescence titration of **H_2L** (10 μM) in HEPES buffer at pH =7.4 by gradual addition of Al^{3+} (0–10 μM) with λem= 478 nm (5/5 slit). Inset: non-linear plot of fluorescence intensity vs. concentration of Al^{3+} ion.

View Article Online
DOI: 10.1039/C6RA21217D

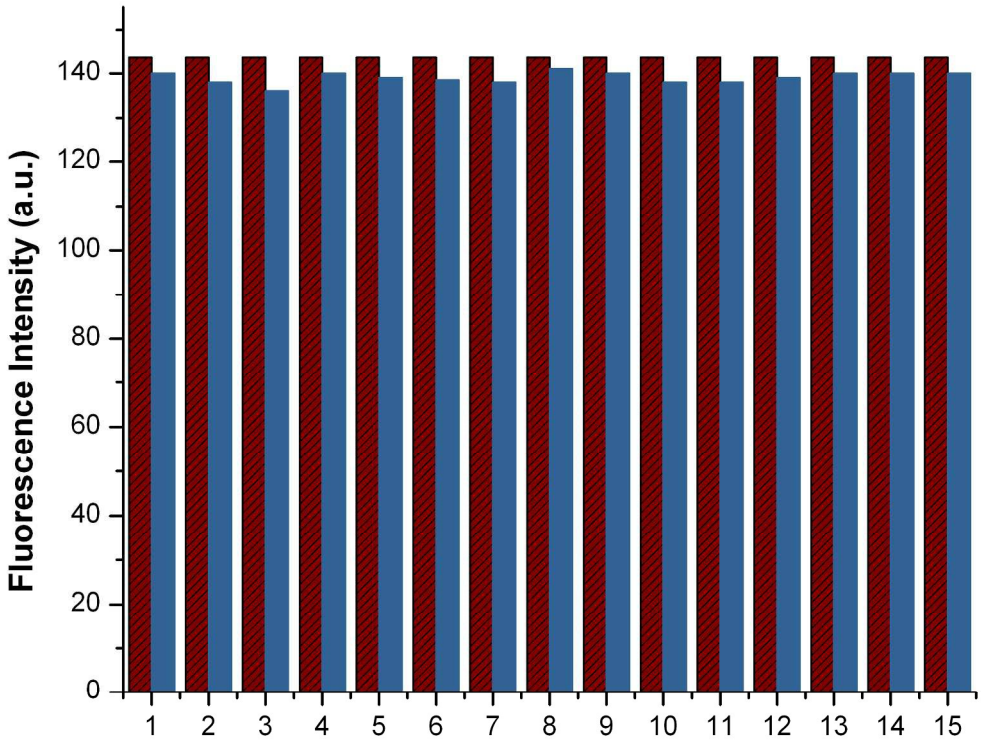

Fig. 5. Relative fluorescence intensity profile of [H_2L-Al^{3+}] system in the presence of different cations in HEPES buffer at pH 7.4. **H_2L**(10 μM) + Al^{3+}(10 μM) + M^{n+}(500 μM), where M^{n+}=(1–Cd^{2+},2–Co^{2+},3–Cr^{3+},4–Cu^{2+},5–Fe^{3+},6–Hg^{2+},7–K^{+},8–Mn^{2+},9–Na^{+},10-Ni^{2+},11–Sn^{2+},12–Zn^{2+},13–Ag^{+},14-Fe^{2+},15–Ca^{2+}).

View Article Online
DOI: 10.1039/C6RA21217D

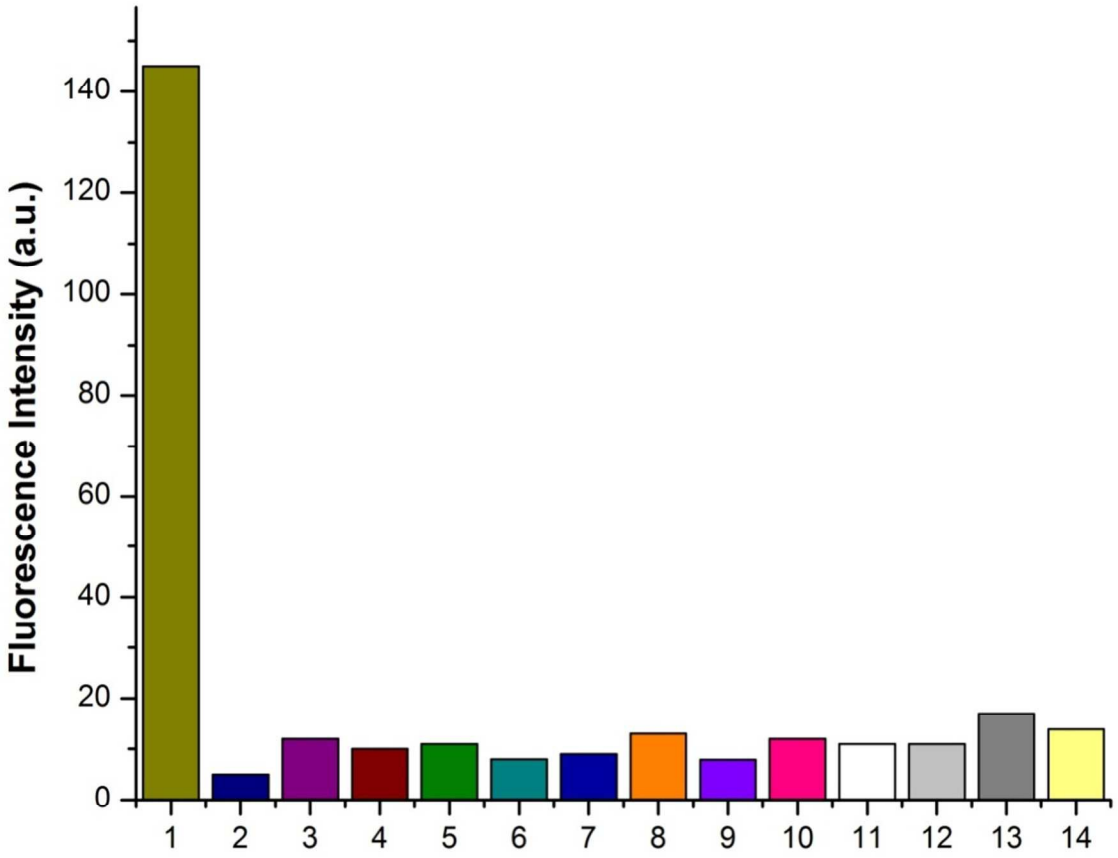

Fig. 6. Relative fluorescence intensity profile of **H_2L** (10 μM) in the presence of various common anions (50 μM) in HEPES buffer at pH 7.4.

1- **H_2L**+Al^{3+}, 2 – 14 **H_2L** + Anions, Anions = 2-$S_2O_3^{2-}$, 3-S^{2-}, 4-SO_3^{2-}, 5- SO_4^{2-}, 6-SCN^-, 7-N_3^-, 8-AsO_4^{3-}, 9-PO_4^{3-}, 10-ClO_4^-, 11-OAc^-, 12-Cl^-, 13-NO_2^-, 14-NO_3^-

View Article Online
DOI: 10.1039/C6RA21217D

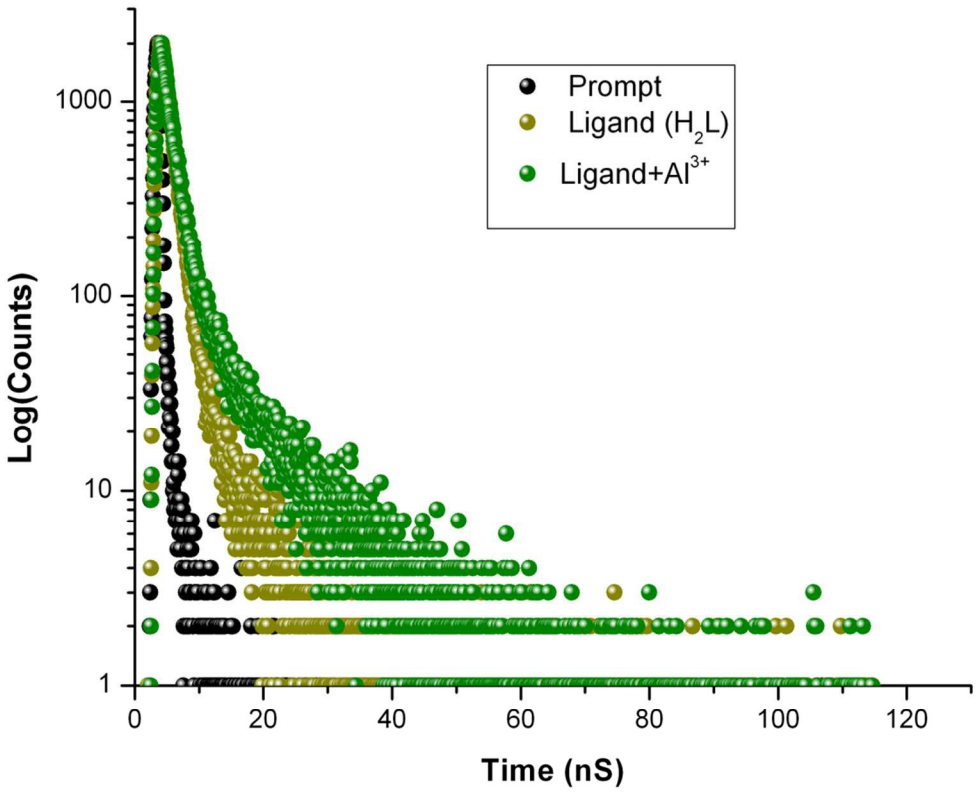

Fig. 7. Time-resolved fluorescence decay curves (logarithm of normalized intensity vs time in ns) of **H_2L** in the absence ( ) and presence ( ) of Al^{3+}ion, ( ) indicates decay curve for the scattered (λex= 478 nm).

View Article Online
DOI: 10.1039/C6RA21217D

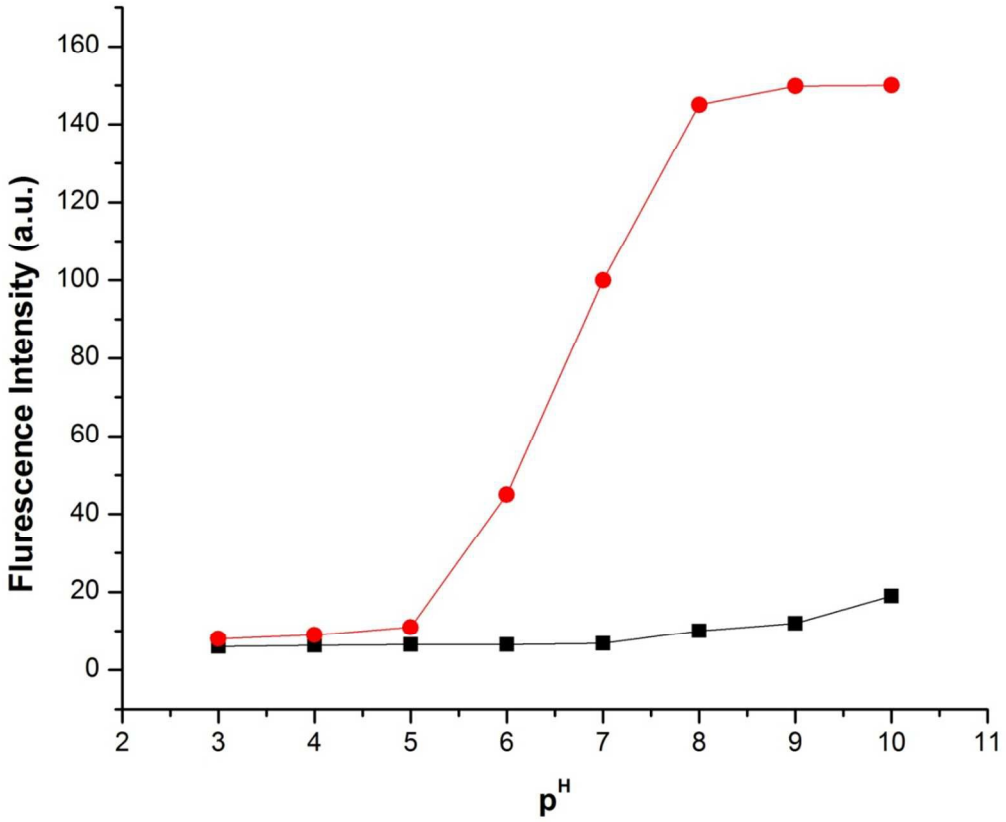

Fig. 8. Fluorescence intensity of **H_2L** (black box; 10 μM) in the absence and presence of Al^{3+}ion (red circle, 10 μM) ion at various pH values in HEPES buffer.

View Article Online
DOI: 10.1039/C6RA21217D

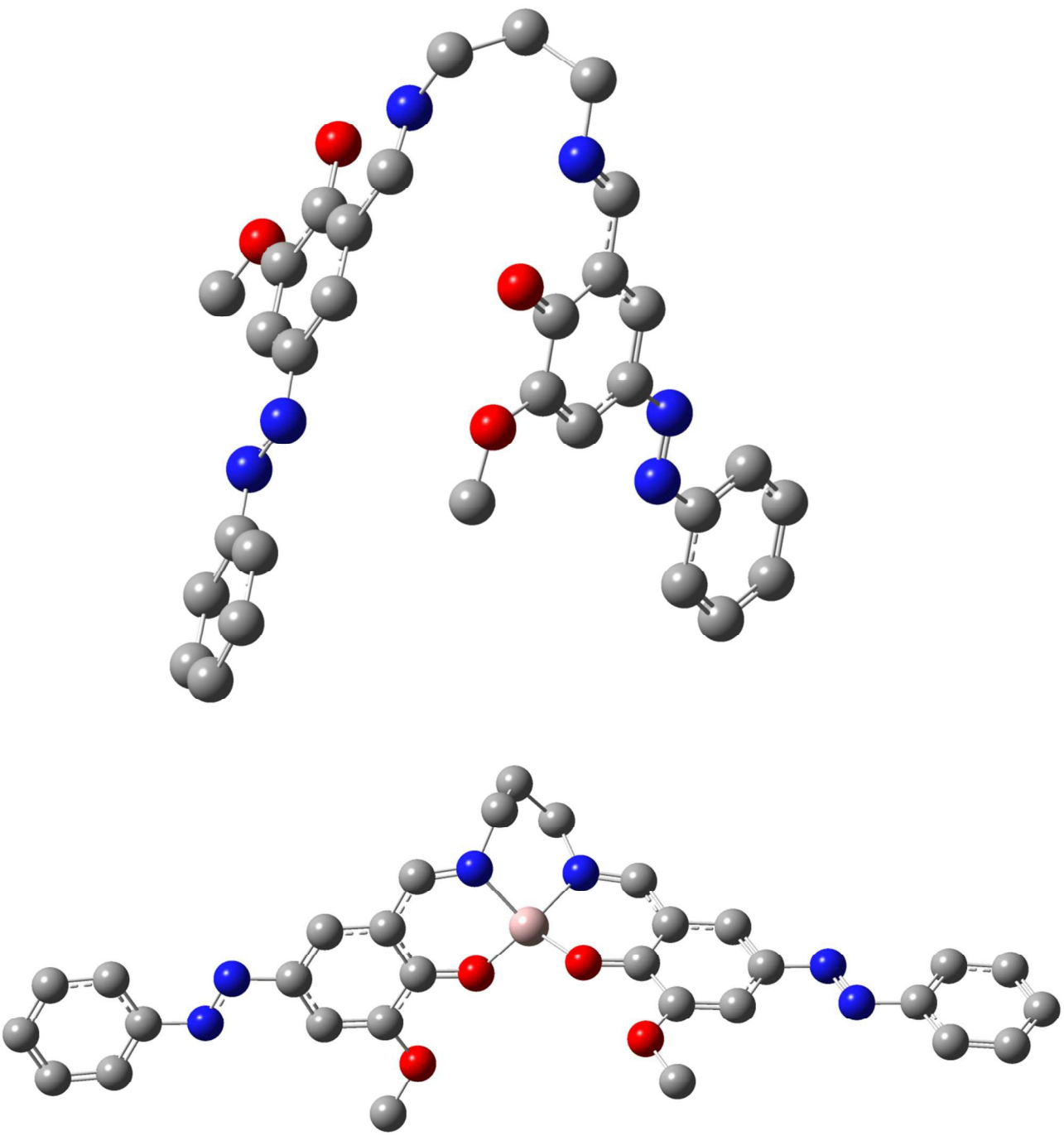

Fig.9. DFT optimized structures of **H_2L** and $[Al(L)]^+$. H-atoms are omitted for clarity.

View Article Online
DOI: 10.1039/C6RA21217D

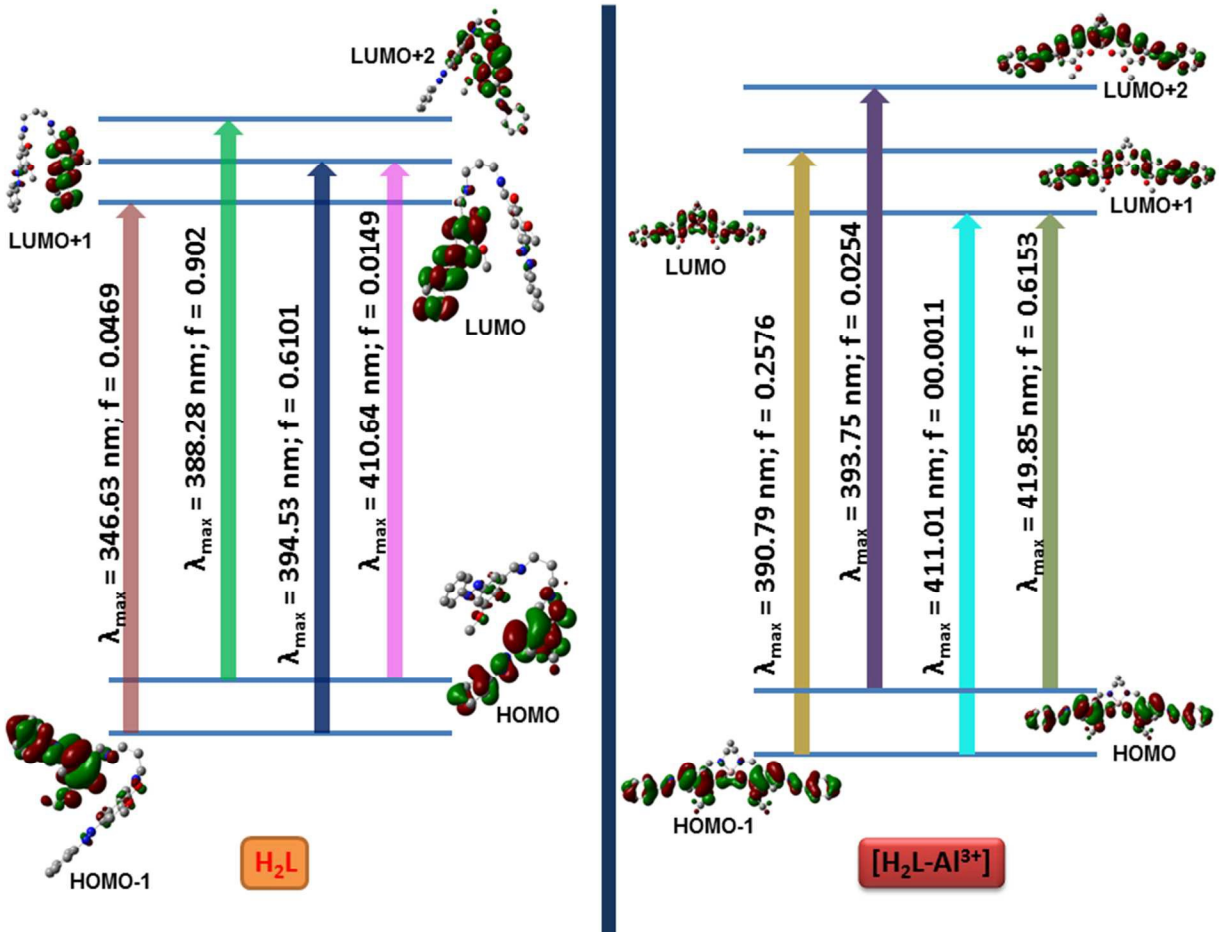

Fig.10. Pictorial representation of key transitions of **H_2L** and $[Al(L)]^+$.

View Article Online
DOI: 10.1039/C6RA21217D

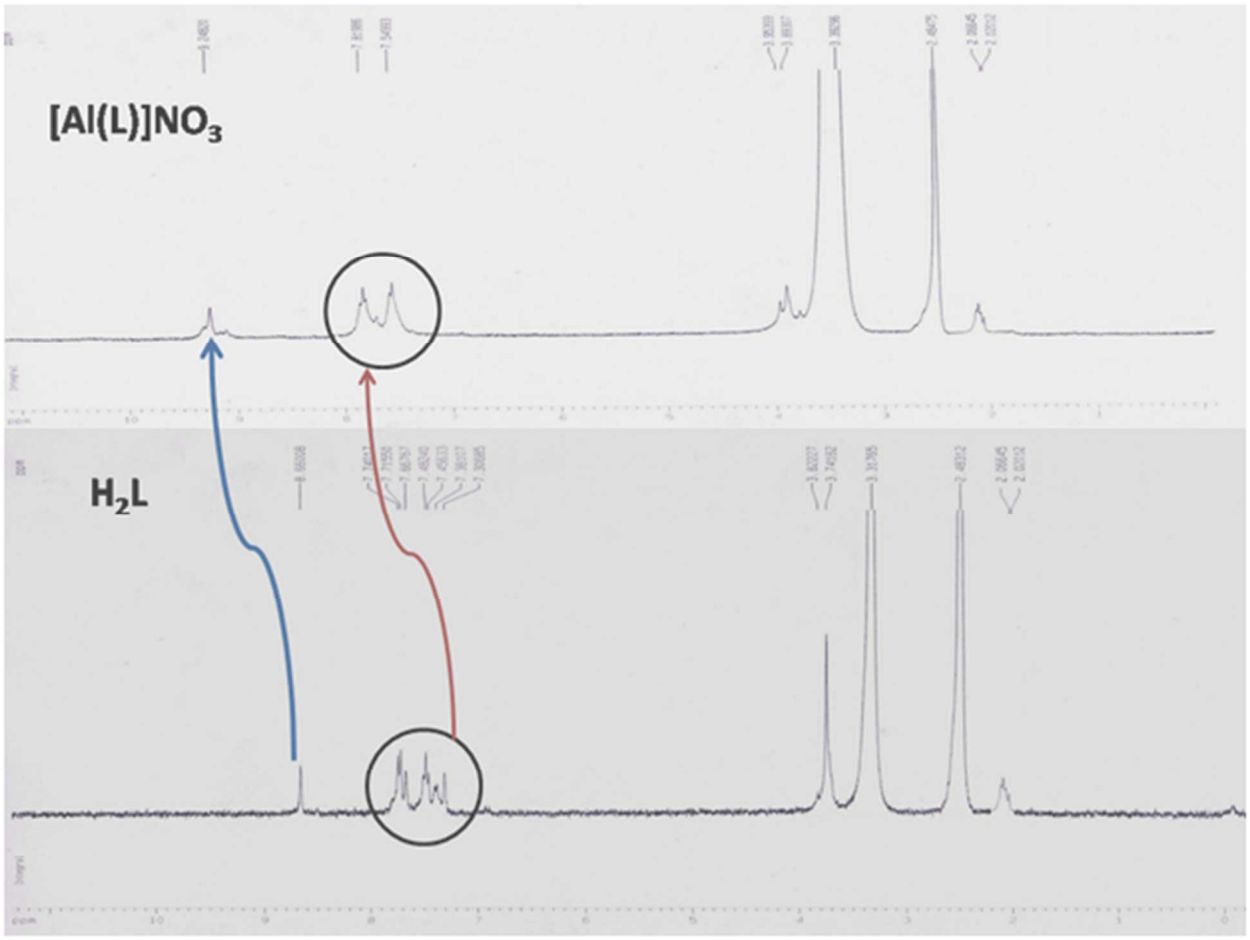

Fig. 11. NMR titration of **H_2L** in presence of 1 eq. of Al^{3+} ion.

View Article Online
DOI: 10.1039/C6RA21217D

Fig. 12. Pictorial representation of Logic Gate.

View Article Online
DOI: 10.1039/C6RA21217D

A Robust Fluorescent Chemo sensor for Aluminium Ion Detection Based on Schiff base Ligand with Azo Arm and Application in Molecular Logic Gate

Saikat Banerjee[a], Paula Brandão[b] and Amrita Saha[a,*]

Herewith, we have reported a new Schiff base chemosensor with azo arm for Al^{3+} ions. The sensor has been well characterized using different techniques like single crystal x-ray, NMR, IR, UV etc. It shows excellent selectivity over other cations and anions. Detection limit of the sensor was found to be 6.93 nM.

View Article Online
DOI: 10.1039/C6RA21217D

Graphical Abstract (Pictogram)

A Robust Fluorescent Chemo sensor for Aluminium Ion Detection Based on Schiff base Ligand with Azo Arm and Application in Molecular Logic Gate

Saikat Banerjee[a], Paula Brandão[b] and Amrita Saha*[a]